COMPACT FINITE DIFFERENCE SCHEME FOR SOME SOBOLEV TYPE EQUATIONS WITH DIRICHLET BOUNDARY CONDITIONS*

Lavanya V Salian and Rathan Samala[1]

Department of Humanities and Sciences, Indian Institute of Petroleum and Energy,
Visakhapatnam 530003, India
Emails: lavanya_vs@iipe.ac.in, rathans.math@iipe.ac.in

Rakesh Kumar

School of Data Science, Indian Institute of Science Education and Research,
Thiruvananthapuram 695551, India;
Department of Mathematics, École Centrale School of Engineering, Mahindra University,
Hyderabad 500043, Telangana, India
Email: rakesh.kumar@mahindrauniversity.edu.in

Abstract

This study aims to construct a stable, high-order compact finite difference method for solving Sobolev-type equations with Dirichlet boundary conditions. Approximation of higher-order mixed derivatives in some specific Sobolev-type equations requires a bigger stencil information. One can approximate such derivatives on compact stencils, which are higher-order accurate and take less stencil information but are implicit and sparse. Spatial derivatives in this work are approximated using the sixth-order compact finite difference method, while temporal derivatives are handled with the explicit forward Euler difference scheme. We examine the accuracy and convergence behavior of the proposed scheme. Using the von Neumann stability analysis, we establish L_2-stability theory for the linear case. We derive conditions under which fully discrete schemes are stable. Also, the amplification factor $\mathcal{C}(\theta)$ is analyzed to ensure the decay property over time. Real parts of $\mathcal{C}(\theta)$ lying on the negative real axis confirm the exponential decay of the solution. A series of numerical experiments were performed to verify the effectiveness of the proposed scheme. These tests include both one-dimensional and two-dimensional cases of advection-free and advection-diffusion flows. They also cover applications to the equal width equation, such as the propagation of a single solitary wave, interactions between two and three solitary waves, undular bore formation, and the Benjamin-Bona-Mahony-Burgers equation.

Mathematics subject classification: 65M06, 65M12.
Key words: High-order compact scheme, Wave propagation, Stability, Equal-width equation, Benjamin-Bona-Mahony-Burgers equation.

1. Introduction

Sobolev-type equations are partial differential equations (PDEs) that feature third-order mixed time and space derivatives. They describe wave motion in media with nonlinear wave steepening, dispersion, and diffusion, making them essential for various scientific and engineering applications. These equations are widely used to model physical phenomena such as

moisture migration in soil [34], fluid flow through fractured rock [4], shear in second-order fluids [39], consolidation of clay [38], and processes in semiconductors [12], providing valuable insights across disciplines including hydrodynamics [13] and thermodynamics [10].

In this paper, we focus on a high-order compact finite difference scheme for solving a class of Sobolev-type equations with a Burgers-type nonlinear term, given by

$$u_t + f(u)_x - \gamma u_{xx} - \delta u_{xxt} = g(x,t), \quad x \in \Omega \subseteq \mathbb{R}, \quad t \in (0,T] \tag{1.1}$$

with initial condition

$$u(x,0) = \omega(x), \quad x \in \Omega, \tag{1.2}$$

and Dirichlet boundary conditions. Here, $f(u)$ represents the nonlinear function, g is a source term, and $\gamma, \delta \geq 0$ are constants. Eq. (1.1) represents various classes of linear and nonlinear PDEs. The study will primarily concentrate on the equal width (EW) and the Benjamin-Bona-Mahony-Burgers (BBMB) equations.

The EW equation, introduced by Morrison *et al.* [24], is a mathematical model that describes one-dimensional wave propagation within nonlinear media, containing dispersive effects, is given by

$$u_t + u u_x = \delta u_{xxt}, \quad x \in \Omega, \quad t \in (0,T]. \tag{1.3}$$

It is presented as an alternative to both the regularized long wave (RLW) and Korteweg-de Vries (KdV) equations, which are also known to model nonlinear dispersive wave phenomena featuring solitary waves that preserve their shape and speed post-interaction. To simulate physical boundary conditions, the EW equation is equipped with the condition $u = 0$ at $x = x_0$ and $x = x_N$, signifying that $u \to 0$ as $x \to \pm\infty$, with boundaries positioned sufficiently far apart initially. This PDE is termed the "equal width equation" due to the fact that, given a specific value of the parameter δ, solitary wave solutions exhibit a consistent width or wavelength across different wave amplitudes. A bore arises when a deeper flow of water moves into a still-water region, particularly when the depth transition has a gentle slope. Experimental findings suggest that if the depth change ratio is below 0.28, the resulting bore exhibits undular characteristics. However, when this ratio exceeds 0.28, at least one wave crest in the bore begins to break [28]. Analytical solutions to the EW equation exist but are confined to specific initial and boundary conditions [17]. However, several numerical methods have been developed to study it, including those found in [9, 14, 20, 21, 31–33].

The EW equation omits dissipation, but it is essential to examine how numerical methods handle dissipative effects alongside nonlinearity and dispersion. Thus, one can consider the inhomogeneous BBMB equation

$$u_t + (1+u)u_x - \gamma u_{xx} - \delta u_{xxt} = g(x,t), \quad x \in \Omega, \quad t \in (0,T], \tag{1.4}$$

which incorporates dissipation through the term γu_{xx}. References [5–7] discuss exact solutions and conservation laws for the BBMB equation. The BBM equation is notable for modeling long-wavelength waves in media like fluids and plasma [1]. Several analytical methods, such as the tanh-coth [15], Exp-function [11,25], and G'/G-expansion techniques [3], have been employed to address generalized BBM and BBM-Burgers equations. Research also includes investigations of solution stability, decay rates [16, 29, 41], and shock profile behavior in two-dimensional cases [40]. Numerical methods, including homotopy perturbation, variational iteration [37], meshless method of radial basis functions [8], B-spline methods [18–20] and finite difference schemes [2], have been used to obtain approximate solutions with verified accuracy.

The objective of this study is to construct a stable, high-order compact finite difference method for solving Sobolev-type equations of the form (1.1) with Dirichlet boundary conditions. Approximation of higher-order mixed derivatives in some specific Sobolev-type equations requires a bigger stencil information. One can approximate such derivatives on compact stencils, which are higher-order accurate and take less stencil information but are implicit and sparse. Spatial derivatives in (1.1) in this work are approximated using the sixth-order compact finite difference method (Compact6), while temporal derivatives are handled with the explicit forward Euler difference scheme. We examine the accuracy and convergence behavior of the proposed scheme. Using the von Neumann stability analysis, we establish L_2-stability theory for the linear case. We derive conditions under which fully discrete schemes (Euler forward time-stepping combined with Compact6 spatial discretization) are stable. Also, the amplification factor $\mathcal{C}(\theta)$ is analyzed to ensure the decay property over time. Real parts of $\mathcal{C}(\theta)$ lying on the negative real axis confirm the exponential decay of the solution. A series of numerical experiments were performed to verify the effectiveness of the proposed scheme. These tests include both one-dimensional and two-dimensional cases of advection-free and advection-diffusion flows. They also cover applications to the equal width equation, such as the propagation of a single solitary wave, interactions between two and three solitary waves, undular bore formation, and the Benjamin-Bona-Mahony-Burgers equation. These cases were examined to confirm the theoretical findings and assess the scheme's accuracy and stability.

We organize the paper as follows. In Section 2, we provide a compact sixth-order finite-difference approximation to spatial first and second-order derivatives involved in Sobolev-type equations in semi- and fully discrete formulations along with the implementation of Dirichlet boundary conditions. In Section 3, we establish certain conditions to prove the stability of the proposed scheme in the linear case, and hence we prove the solution is bounded in semi- and fully-discrete formulations. In Section 4, we present numerical results to some examples in one and two-dimensions to validate the theoretical results. Finally, we provide some conclusions in Section 5.

2. Compact Sixth-Order Scheme

In this section, we aim to develop a numerical scheme with sixth-order accuracy in space and first-order accuracy in time to approximate the solution of Eq. (1.1). We define the spatial domain $\Omega = \{x \mid a \leq x \leq b\}$, where a and b are constants, and discretize it into N equally spaced intervals so that $x_j = a + jh$ for $j = 1, 2, \ldots, N$, where $h = (b-a)/N$ represents the spatial step size. In the temporal direction, we divide the interval $[0, T]$ into M uniform time steps, each of size $\tau = T/M$. The discrete-time levels are then given by $t^n = n\tau$, where n is the time index. Let u_j^n be the approximate solution at (x_j, t^n). Define u'_j and u''_j as approximations to derivatives $\partial u/\partial x$ and $\partial^2 u/\partial x^2$ at x_j, respectively.

Consider the one-dimensional Sobolev-type equations (1.1) in the quasi-linear form

$$u_t + f'(u)u_x - \gamma u_{xx} - \delta u_{xxt} = \mathrm{g}(x,t). \tag{2.1}$$

To approximate the first and second derivatives, u_x and u_{xx}, at each grid point, we apply a sixth-order compact finite difference scheme on a linear cell-node grid as presented in [22]. For the first derivative, the formulation is as follows:

$$\frac{1}{3}u'_{j-1} + u'_j + \frac{1}{3}u'_{j+1}$$

$$= \frac{14}{9} \frac{u_{j+1} - u_{j-1}}{2h} + \frac{1}{9} \frac{u_{j+2} - u_{j-2}}{4h}$$

$$= \frac{1}{h} \left(-\frac{1}{36} u_{j-2} - \frac{7}{9} u_{j-1} + \frac{7}{9} u_{j+1} + \frac{1}{36} u_{j+2} \right), \quad 1 \le j \le N. \tag{2.2}$$

The local truncation error of the scheme is $-u_j^{(7)}(x)h^6/1260 + \mathcal{O}(h^8)$. The Eq. (2.2) can be represented in matrix form as

$$\mathcal{A}_1 \mathbf{u}' = \frac{1}{h} \mathcal{B}_1 \mathbf{u},$$

$$\mathbf{u}' = \frac{1}{h} \mathcal{D}_1 \mathbf{u}, \tag{2.3}$$

where

$$\mathbf{u}' = (u_1', u_2', \ldots, u_N')^\top, \quad \mathbf{u} = (u_1, u_2, \ldots, u_N)^\top,$$

$\mathcal{D}_1 = \mathcal{A}_1^{-1} \mathcal{B}_1$ is the first derivative differentiation matrix and $\mathcal{A}_1, \mathcal{B}_1 \in \mathbb{R}^{N \times N}$ are tri- and penta-diagonal matrices given by

$$\mathcal{A}_1 = \begin{pmatrix} 1 & \frac{1}{3} & 0 & \cdots & \cdots & \cdots & 0 \\ \frac{1}{3} & 1 & \frac{1}{3} & \cdots & \cdots & \cdots & 0 \\ 0 & \frac{1}{3} & 1 & \cdots & \cdots & \cdots & 0 \\ \vdots & \vdots & \vdots & \ddots & \vdots & \vdots & \vdots \\ 0 & 0 & 0 & \cdots & \cdots & 1 & \frac{1}{3} \\ 0 & 0 & 0 & \cdots & \cdots & \frac{1}{3} & 1 \end{pmatrix},$$

$$\mathcal{B}_1 = \begin{pmatrix} 0 & \frac{7}{9} & \frac{1}{36} & 0 & \cdots & \cdots & 0 \\ -\frac{7}{9} & 0 & \frac{7}{9} & \frac{1}{36} & \cdots & \cdots & 0 \\ -\frac{1}{36} & -\frac{7}{9} & 0 & \frac{7}{9} & \frac{1}{36} & \cdots & 0 \\ 0 & -\frac{1}{36} & -\frac{7}{9} & 0 & \frac{7}{9} & \cdots & 0 \\ \vdots & \vdots & \vdots & \vdots & \ddots & \vdots & \vdots \\ 0 & \cdots & 0 & -\frac{1}{36} & -\frac{7}{9} & 0 & \frac{7}{9} \\ 0 & \cdots & 0 & 0 & -\frac{1}{36} & -\frac{7}{9} & 0 \end{pmatrix}. \tag{2.4}$$

For the second derivative, we utilize the following expression:

$$\frac{2}{11} u_{j-1}'' + u_j'' + \frac{2}{11} u_{j+1}''$$

$$= \frac{12}{11} \frac{u_{j+1} - 2u_j + u_{j-1}}{h^2} + \frac{3}{11} \frac{u_{j+2} - 2u_j + u_{j-2}}{4h^2}$$

$$= \frac{1}{h^2} \left(\frac{3}{44} u_{j-2} + \frac{12}{11} u_{j-1} - \frac{51}{22} u_j + \frac{12}{11} u_{j+1} + \frac{3}{44} u_{j+2} \right). \tag{2.5}$$

The local truncation error of the scheme is $-23u_j^{(8)}(x)h^6/55440 + \mathcal{O}(h^8)$. In matrix form, Eq. (2.5) becomes

$$
\begin{aligned}
\mathcal{A}_2\mathbf{u}'' &= \frac{1}{h^2}\mathcal{B}_2\mathbf{u}, \\
\mathbf{u}'' &= \frac{1}{h^2}\mathcal{D}_2\mathbf{u},
\end{aligned}
\tag{2.6}
$$

where

$$
\mathbf{u}'' = (u_1'', u_2'', \ldots, u_N'')^\top,
$$

$\mathcal{D}_2 = \mathcal{A}_2^{-1}\mathcal{B}_2$ is the second derivative differentiation matrix and $\mathcal{A}_2, \mathcal{B}_2 \in \mathbb{R}^{N\times N}$ are tri- and penta-diagonal matrices given by

$$
\mathcal{A}_2 = \begin{pmatrix}
1 & \frac{2}{11} & 0 & \cdots & \cdots & \cdots & 0 \\
\frac{2}{11} & 1 & \frac{2}{11} & \cdots & \cdots & \cdots & 0 \\
0 & \frac{2}{11} & 1 & \cdots & \cdots & \cdots & 0 \\
\vdots & \vdots & \vdots & \ddots & \vdots & \vdots & \vdots \\
0 & 0 & 0 & \cdots & \cdots & 1 & \frac{2}{11} \\
0 & 0 & 0 & \cdots & \cdots & \frac{2}{11} & 1
\end{pmatrix},
$$

$$
\mathcal{B}_2 = \begin{pmatrix}
-\frac{51}{22} & \frac{12}{11} & \frac{3}{44} & 0 & \cdots & \cdots & 0 \\
\frac{12}{11} & -\frac{51}{22} & \frac{12}{11} & \frac{3}{44} & \cdots & \cdots & 0 \\
\frac{3}{44} & \frac{12}{11} & -\frac{51}{22} & \frac{12}{11} & \frac{3}{44} & \cdots & 0 \\
0 & \frac{3}{44} & \frac{12}{11} & -\frac{51}{22} & \frac{12}{11} & \cdots & 0 \\
\vdots & \vdots & \vdots & \vdots & \ddots & \vdots & \vdots \\
0 & \cdots & 0 & \frac{3}{44} & \frac{12}{11} & -\frac{51}{22} & \frac{12}{11} \\
0 & \cdots & 0 & 0 & \frac{3}{44} & \frac{12}{11} & -\frac{51}{22}
\end{pmatrix}.
\tag{2.7}
$$

The derivatives u_x and u_{xx} are approximated at the grid points by the vectors $\mathbf{u}'$ and $\mathbf{u}''$, respectively, as defined by Eqs. (2.3) and (2.6). With these approximations, Eq. (2.1) can be reformulated as

$$
\mathbf{u}_t + \operatorname{diag}\big(f'(\mathbf{u})\big)\mathbf{u}' - \gamma\mathbf{u}'' - \delta\mathbf{u}_t'' \approx \mathbf{g}, \quad t > 0, \tag{2.8}
$$

where

$$
\begin{aligned}
f'(\mathbf{u}) &= \big(f'(u_1), f'(u_2), \ldots, f'(u_N)\big)^\top, \\
\mathbf{g} &= \big(g(x_1, t), g(x_2, t), \ldots, g(x_N, t)\big)^\top.
\end{aligned}
$$

By substituting the discrete forms, we arrive at the expression

$$\left(I - \frac{\delta}{h^2}\mathcal{D}_2\right)\mathbf{u}_t = -\frac{1}{h}\text{diag}\big(f'(\mathbf{u})\big)\mathcal{D}_1\mathbf{u} + \frac{\gamma}{h^2}\mathcal{D}_2\mathbf{u} + \mathbf{g}. \qquad (2.9)$$

To advance the solution in time, we apply the forward Euler method for the time derivative, resulting in the matrix equation

$$\left(I - \frac{\delta}{h^2}\mathcal{D}_2\right)\mathbf{U}^{n+1} = \left(I - \frac{\tau}{h}\text{diag}\big(f'(\mathbf{U}^n)\big)\mathcal{D}_1 + \frac{\tau\gamma - \delta}{h^2}\mathcal{D}_2\right)\mathbf{U}^n + \tau\mathbf{g}^n, \qquad (2.10)$$

where $\mathbf{U}^n = (u_1^n, u_2^n, \ldots, u_N^n)^\top$ represents the solution vector at time level $t = n\tau$.

At the initial time level, $n = 0$, the vector $\mathbf{U}^0$ is determined from the initial condition given in Eq. (1.2). To obtain $\mathbf{U}^{n+1}$ at time $t = (n+1)\tau$, we solve the linear system in Eq. (2.10). Since $\mathbf{U}^n$ at time $t = n\tau$ is already known, the right-hand side of the Eq. (2.10) can be computed directly, allowing the next time step solution vector $\mathbf{U}^{n+1}$ to be obtained. Using the Taylor expansion in (2.10), we get the following.

Theorem 2.1. *Assume that the solution u of (2.1) belongs to the space $C_2^8((a,b) \times [0,T])$. Then, as the time step $\tau \to 0$ and the spatial step $h \to 0$, the Compact6 method (2.10) achieves a local truncation error of order $\mathcal{O}(\tau + h^6)$.*

Boundary conditions: Many computational problems in physics involve non-periodic domains, requiring non-periodic boundary conditions. Therefore, specialized boundary schemes are necessary to accurately compute physical quantities near the edges of the domain. Finite-difference methods are typically used on grids where boundaries align with grid points. The solution is specified at the first and last points, and the governing equations are not solved at these boundaries. Since high-order schemes require neighbouring points that are absent near boundaries, reduced-order or biased schemes are applied at boundary-adjacent points, as they lack sufficient neighbours to support the same numerical approach used in the interior of the grid.

The values for u_j^n, for $j = 1, 2, N-1, N$ are obtained using the boundary condition and hence need to be treated as known quantities. The computation of the spatial derivatives u_3' and u_{N-2}' is nontrivial because standard centered finite difference formulas cannot be applied directly near the boundaries. In particular, for a sixth-order accurate centered finite difference approximation of the first derivative, one typically requires symmetric stencils that span three grid points on either side of the evaluation point. However, at the grid points x_3 and x_{N-2}, such symmetric stencils would require access to values outside the computational domain, which are not available.

To address this issue, we use one-sided finite difference formulas that are specially constructed to maintain sixth-order accuracy despite the lack of symmetry in the stencil. These formulas are derived by expanding the solution $u(x)$ in a Taylor series about the point of interest and determining coefficients that yield a truncation error of $\mathcal{O}(h^6)$.

For example, around the point x_3, we consider Taylor series expansions of nearby grid values: As an illustration, to derive a high-order one-sided approximation at the point x_3, we express the nearby function values u_j, for $j = 1, 2, \ldots, 6$, using their Taylor series expansions around that point. These expansions can be compactly written in the form

$$u_j = u + jh\,u' + \frac{(jh)^2}{2!}u'' + \frac{(jh)^3}{3!}u^{(3)} + \frac{(jh)^4}{4!}u^{(4)} + \frac{(jh)^5}{5!}u^{(5)} + \mathcal{O}(h^6), \quad j = 1, 2, \ldots, 6.$$

The first derivative at x_3 is then given by

$$u'_3 = u'(x + 3h) = u' + 3h\,u'' + \frac{9h^2}{2}u^{(3)} + \frac{27h^3}{6}u^{(4)} + \frac{81h^4}{24}u^{(5)} + \mathcal{O}(h^5).$$

To obtain a one-sided finite difference formula of the form

$$u'_3 \approx \frac{1}{h}(a_1u_1 + a_2u_2 + a_3u_3 + a_4u_4 + a_5u_5 + a_6u_6),$$

we substitute the Taylor expansions into the linear combination and match terms with the Taylor expansion of u'_3. This leads to the following system of equations for the coefficients $a_1, a_2, \ldots, a_6$:

$$a_1 + a_2 + a_3 + a_4 + a_5 + a_6 = 0,$$
$$a_1(1) + a_2(2) + a_3(3) + a_4(4) + a_5(5) + a_6(6) = 1,$$
$$a_1\left(\frac{1}{2}\right) + a_2(2) + a_3\left(\frac{9}{2}\right) + a_4(8) + a_5\left(\frac{25}{2}\right) + a_6(18) = 3,$$
$$a_1\left(\frac{1}{6}\right) + a_2\left(\frac{4}{3}\right) + a_3\left(\frac{9}{2}\right) + a_4\left(\frac{64}{6}\right) + a_5\left(\frac{125}{6}\right) + a_6(36) = \frac{9}{2},$$
$$a_1\left(\frac{1}{24}\right) + a_2\left(\frac{1}{3}\right) + a_3\left(\frac{27}{8}\right) + a_4\left(\frac{256}{24}\right) + a_5\left(\frac{625}{24}\right) + a_6\left(\frac{1296}{24}\right) = \frac{9}{2},$$
$$a_1\left(\frac{1}{120}\right) + a_2\left(\frac{2}{15}\right) + a_3\left(\frac{81}{40}\right) + a_4\left(\frac{1024}{120}\right) + a_5\left(\frac{3125}{120}\right) + a_6\left(\frac{7776}{120}\right) = \frac{81}{24}.$$

After solving the resulting system, we obtain

$$a_1 = \frac{1}{20}, \quad a_2 = -\frac{1}{2}, \quad a_3 = -\frac{1}{3}, \quad a_4 = 1, \quad a_5 = -\frac{1}{4}, \quad a_6 = \frac{1}{30}.$$

Thus, the sixth-order one-sided finite difference approximation of the first derivative at x_3 is

$$u'_3 = \frac{1}{h}\left(\frac{1}{20}u_1 - \frac{1}{2}u_2 - \frac{1}{3}u_3 + u_4 - \frac{1}{4}u_5 + \frac{1}{30}u_6\right) + \mathcal{O}(h^6).$$

Similarly, the computation of u'_{N-2} near the right boundary is performed using a sixth-order one-sided stencil that involves grid points x_{N-5} through x_N. By performing a Taylor series expansion about x_{N-2} and solving the corresponding coefficient system, we obtain the mirror-image formula

$$u'_{N-2} = \frac{1}{h}\left(-\frac{1}{20}u_N + \frac{1}{2}u_{N-1} + \frac{1}{3}u_{N-2} - u_{N-3} + \frac{1}{4}u_{N-4} - \frac{1}{30}u_{N-5}\right) + \mathcal{O}(h^6).$$

For $\mathbf{u}^n = (u_3^n, u_4^n, \ldots, u_{N-3}^n, u_{N-2}^n)^\top$, the first derivative in the matrix form is given by

$$\mathbf{A}_1\mathbf{u}' = \frac{1}{h}\left(\mathbf{B}_1\mathbf{u}^n + \mathbf{C}_1^n\right), \tag{2.11}$$

where, the matrices $\mathbf{A}_1, \mathbf{B}_1 \in \mathbb{R}^{(N-4)\times(N-4)}$ and column vector $\mathbf{C}_1^n \in \mathbb{R}^{(N-4)\times 1}$, are given by

$$
\mathbf{A}_1 = \begin{pmatrix}
1 & 0 & 0 & \cdots & 0 & 0 & 0 & 0 \\
\frac{1}{3} & 1 & \frac{1}{3} & \ddots & & & & 0 \\
0 & \frac{1}{3} & 1 & \frac{1}{3} & \ddots & & & 0 \\
\vdots & \ddots & \ddots & \ddots & \ddots & \ddots & & \vdots \\
0 & & \ddots & \frac{1}{3} & 1 & \frac{1}{3} & 0 & 0 \\
0 & & & \ddots & \frac{1}{3} & 1 & \frac{1}{3} & 0 \\
0 & & & & \ddots & \frac{1}{3} & 1 & \frac{1}{3} \\
0 & 0 & 0 & \cdots & 0 & 0 & 0 & 1
\end{pmatrix},
$$

$$
\mathbf{B}_1 = \begin{pmatrix}
-\frac{1}{3} & 1 & -\frac{1}{4} & \frac{1}{30} & \cdots & 0 & 0 & 0 \\
-\frac{7}{9} & 0 & \frac{7}{9} & \frac{1}{36} & \ddots & & & 0 \\
-\frac{1}{36} & -\frac{7}{9} & 0 & \frac{7}{9} & \frac{1}{36} & \ddots & & 0 \\
0 & -\frac{1}{36} & -\frac{7}{9} & 0 & \frac{7}{9} & \frac{1}{36} & \ddots & 0 \\
\vdots & \ddots & \ddots & \ddots & \ddots & \ddots & \ddots & \vdots \\
0 & & \ddots & -1 & -\frac{7}{9} & 0 & \frac{7}{9} & \frac{1}{36} \\
0 & & & 0 & -\frac{1}{36} & -\frac{7}{9} & 0 & \frac{7}{9} \\
0 & 0 & 0 & \cdots & -\frac{1}{30} & \frac{1}{4} & -1 & \frac{1}{3}
\end{pmatrix},
$$

(2.12)

$$
\mathbf{C}_1^n = \left(\frac{1}{20}u_1^n - \frac{1}{2}u_2^n, -\frac{1}{36}u_2^n, 0, \cdots, 0, \frac{1}{36}u_{N-1}^n, -\frac{1}{20}u_N^n + \frac{1}{2}u_{N-1}^n \right)^\top. \tag{2.13}
$$

Similarly, the one-sided finite difference approximation of sixth-order for the second derivatives at the grid points x_3, and x_{N-2} are given by

$$
\begin{aligned}
u_3'' &= \frac{1}{h^2}\left[-\frac{1}{12}u_1 + \frac{4}{3}u_2 - \frac{5}{2}u_3 + \frac{4}{3}u_4 - \frac{1}{12}u_5 \right], \\
u_{N-2}'' &= \frac{1}{h^2}\left[-\frac{1}{12}u_N + \frac{4}{3}u_{N-1} - \frac{5}{2}u_{N-2} + \frac{4}{3}u_{N-3} - \frac{1}{12}u_{N-4} \right].
\end{aligned}
\tag{2.14}
$$

The second derivative in the matrix form is given by

$$
\mathbf{A}_2 \mathbf{u}'' = \frac{1}{h^2}\left(\mathbf{B}_2 \mathbf{u}^n + \mathbf{C}_2^n \right), \tag{2.15}
$$

where, the matrix $\mathbf{A}_2$, $\mathbf{B}_2$ and column vector $\mathbf{C}_2^n$, are given by

$$\mathbf{A}_2 = \begin{pmatrix} 1 & 0 & 0 & \cdots & 0 & 0 & 0 & 0 \\ \frac{2}{11} & 1 & \frac{2}{11} & \ddots & & & & 0 \\ 0 & \frac{2}{11} & 1 & \frac{2}{11} & \ddots & & & 0 \\ \vdots & \ddots & \ddots & \ddots & \ddots & \ddots & & \vdots \\ 0 & & \ddots & \frac{2}{11} & 1 & \frac{2}{11} & 0 & 0 \\ 0 & & & \ddots & \frac{2}{11} & 1 & \frac{2}{11} & 0 \\ 0 & & & & \ddots & \frac{2}{11} & 1 & \frac{2}{11} \\ 0 & 0 & 0 & \cdots & 0 & 0 & 0 & 1 \end{pmatrix},$$

$$\mathbf{B}_2 = \begin{pmatrix} -\frac{5}{2} & \frac{4}{3} & -\frac{1}{12} & 0 & \cdots & 0 & 0 & 0 \\ \frac{12}{11} & -\frac{51}{22} & \frac{12}{11} & \frac{3}{44} & \ddots & & & 0 \\ \frac{3}{44} & \frac{12}{11} & -\frac{51}{22} & \frac{12}{11} & \frac{3}{44} & \ddots & & 0 \\ 0 & \frac{3}{44} & \frac{12}{11} & -\frac{51}{22} & \frac{12}{11} & \frac{3}{44} & \ddots & 0 \\ \vdots & \ddots & \ddots & \ddots & \ddots & \ddots & \ddots & \vdots \\ 0 & & \ddots & \frac{3}{44} & \frac{12}{11} & -\frac{51}{22} & \frac{12}{11} & \frac{3}{44} \\ 0 & & & 0 & \frac{3}{44} & \frac{12}{11} & -\frac{51}{22} & \frac{12}{11} \\ 0 & 0 & 0 & \cdots & 0 & -\frac{1}{12} & \frac{4}{3} & -\frac{5}{2} \end{pmatrix},$$

$$\mathbf{C}_2^n = \left(-\frac{1}{12}u_1^n + \frac{4}{3}u_2^n, \frac{3}{44}u_2^n, 0, \cdots, 0, \frac{3}{44}u_{N-1}^n, -\frac{1}{12}u_N^n + \frac{4}{3}u_{N-1}^n \right)^\top. \tag{2.17}$$

Thus, the method (2.10) now takes the form

$$\left(I - \frac{\delta}{h^2}\mathbf{A}_2^{-1}\mathbf{B}_2 \right)\mathbf{u}_t$$
$$= -\frac{1}{h}\mathrm{diag}\big(f'(\mathbf{u}^n)\big)\mathbf{A}_1^{-1}\mathbf{B}_1\mathbf{u}^n + \frac{\gamma}{h^2}\mathbf{A}_2^{-1}\mathbf{B}_2\mathbf{u}^n + \mathbf{g}^n$$
$$+ \frac{\delta}{h^2}\mathbf{A}_2^{-1}\mathbf{C}_2^{n+1} - \frac{1}{h}\mathrm{diag}\big(f'(\mathbf{u}^n)\big)\mathbf{A}_1^{-1}\mathbf{C}_1^n + \frac{\gamma}{h^2}\mathbf{A}_2^{-1}\mathbf{C}_2^n, \tag{2.18}$$
$$\big(h^2 I - \delta\mathbf{A}_2^{-1}\mathbf{B}_2\big)\mathbf{u}_t$$
$$= -h\,\mathrm{diag}\big(f'(\mathbf{u}^n)\big)\mathbf{A}_1^{-1}\mathbf{B}_1\mathbf{u}^n + \gamma\mathbf{A}_2^{-1}\mathbf{B}_2\mathbf{u}^n + h^2\mathbf{g}^n$$
$$+ \delta\mathbf{A}_2^{-1}\mathbf{C}_2^{n+1} - h\,\mathrm{diag}\big(f'(\mathbf{u}^n)\big)\mathbf{A}_1^{-1}\mathbf{C}_1^n + \gamma\mathbf{A}_2^{-1}\mathbf{C}_2^n.$$

(2.16)

For the time derivative, we apply the forward Euler method, leading to the matrix equation

$$
\left(I - \frac{\delta}{h^2}\mathbf{A}_2^{-1}\mathbf{B}_2\right)\mathbf{U}^{n+1}
$$
$$
= \left(I - \frac{\tau}{h}\mathrm{diag}\big(f'(\mathbf{U}^n)\big)\mathbf{A}_1^{-1}\mathbf{B}_1 + \frac{1}{h^2}(\tau\gamma - \delta)\mathbf{A}_2^{-1}\mathbf{B}_2\right)\mathbf{U}^n + \tau\mathbf{g}^n
$$
$$
+ \frac{\delta}{h^2}\mathbf{A}_2^{-1}\mathbf{C}_2^{n+1} - \frac{\tau}{h}\mathrm{diag}\big(f'(\mathbf{u}^n)\big)\mathbf{A}_1^{-1}\mathbf{C}_1^n + \frac{1}{h^2}(\tau\gamma - \delta)\mathbf{A}_2^{-1}\mathbf{C}_2^n, \qquad (2.19)
$$

where the approximate solution vector takes the form $\mathbf{U}^n = (u_3^n, u_4^n, \cdots, u_{N-3}^n, u_{N-2}^n)^\top$. The extension of the present scheme to the two-dimensional case is carried out in a dimension-by-dimension manner for spatial discretization.

3. Error Analysis

In this section, we perform a stability analysis of the Compact6 method, which is detailed out in Section 2. This is achieved through von-Neumann analysis, focusing specifically on a Sobolev-type equation governed by Eq. (1.1), where we assume $f(u)$ is linear and g is zero. The primary equation for this analysis is

$$
u_t + \alpha u_x = \gamma u_{xx} + \delta u_{xxt}, \quad (x,t) \in (0,b) \times (0,T], \qquad (3.1)
$$

where α is a given real number. Given the linearity of the problem, it is sufficient to consider a single Fourier mode for simplification

$$
u_j(t) = \hat{u}(t)e^{ij\theta}, \qquad (3.2)
$$

where $\theta = \omega h$, ω denotes the wave number and $i = \sqrt{-1}$. By substituting this Fourier mode into the Compact6 method's approximations for the first and second derivatives, we replace u_x and u_{xx} in Eq. 3.1, yielding an ordinary differential equation

$$
\frac{du_j}{dt} = \mathcal{C}(\theta)u_j, \qquad (3.3)
$$

which is the semi-discrete form of (3.1). Here, $\mathcal{C}(\theta)$ is identified as the amplification factor.

Substituting (3.2) into the expression (2.2) of the first derivative of the Compact6 method, we get

$$
\mathbf{u}_j' = \frac{i}{9h}\left[\frac{14\sin(\theta) + \sin(2\theta)/2}{1 + 2\cos(\theta)/3}\right]u_j(t)
$$
$$
= \frac{i}{6h}\left[\frac{28\sin(\theta) + \sin(2\theta)}{3 + 2\cos(\theta)}\right]u_j(t), \quad j = 3, 4, \ldots, N-2, \qquad (3.4)
$$

similarly, substituting (3.2) into the expression (2.5) of the second derivative of the Compact6 method, we get

$$
\mathbf{u}_j'' = \frac{1}{11h^2}\left[\frac{24\cos(\theta) + 3\cos(2\theta)/2 - 51/2}{1 + 4\cos(\theta)/11}\right]u_j(t)
$$
$$
= \frac{1}{2h^2}\left[\frac{48\cos(\theta) + 3\cos(2\theta) - 51}{11 + 4\cos(\theta)}\right]u_j(t), \quad j = 3, 4, \ldots, N-2. \qquad (3.5)
$$

Upon substituting these expressions in (3.1), we get

$$(u_j)_t - \delta(\mathbf{u}_j'')_t = -\alpha \mathbf{u}_j' + \gamma \mathbf{u}_j'', \tag{3.6}$$

and we arrive at the semi-discrete form (3.3), where the amplification factor takes the form

$$\mathcal{C}(\theta) = \frac{\gamma P/(2h^2) - i\alpha Q/(6h)}{1 - \delta P/(2h^2)}, \tag{3.7}$$

where P and Q are defined in (3.12).

Theorem 3.1. *Suppose the initial data u_0 is bounded. Then, for each $j = 1, \ldots, N$, the solution u_j of the semi-discrete system (3.3) satisfies the following inequality:*

$$\|u(t)\|_\infty \leq e^{\Re(\mathcal{C}(\theta))t} \|u_0\|_\infty, \quad t \in [0, T], \tag{3.8}$$

where $\Re(\mathcal{C}(\theta))$ is the real part of $\mathcal{C}(\theta)$.

Proof. Integrating the Eq. (3.3) over the time interval $[0, t]$. At $t = 0$, let $u_j(0) = u_0(x_j)$, we have

$$\int_{u_0(x_j)}^{u_j(t)} \frac{du_j}{u_j} = \int_0^t \mathcal{C}(\theta) dt.$$

On simplification, we get

$$u_j(t) = e^{\mathcal{C}(\theta)t} u_0(x_j).$$

By taking the modulus on both sides, we obtain

$$|u_j(t)| \leq e^{\Re(\mathcal{C}(\theta))t} \|u_0\|_\infty.$$

This inequality holds for every $j = 1, \ldots, N$, thus establishing the desired result. $\square$

Upon applying the forward Euler scheme to Eq. (3.3), we derive the expression for the fully discrete scheme given by

$$u_j^{n+1} = \mathcal{L}(\theta) u_j^n, \tag{3.9}$$

where $\mathcal{L}(\theta)$ is given by

$$\mathcal{L}(\theta) = \frac{1 + (\gamma\tau - \delta)P/(2h^2) - i\alpha\tau Q/(6h)}{1 - \delta P/(2h^2)}, \tag{3.10}$$

where P and Q are defined in (3.12).

In the context of von Neumann stability analysis, the amplification factor is generally expected to stay within a limit of 1. Nevertheless, this condition can be relaxed to $1 + C\tau$, where C is a positive constant [23, 36]. The following theorem presents L_2-stability estimates for the method proposed, specifically when applied to the linear equation (3.1).

Theorem 3.2. *The Compact6 method applied to Eq. (3.1) with the forward Euler method for time discretization remains stable if there exists a constant $C > 0$ such that*

$$\tau \leq \frac{2\big(1 - \delta P/(2h^2)\big)\big(C - C\delta P/(2h^2) - \gamma P/(2h^2)\big)}{\big(\gamma^2 P^2/(4h^4) + \alpha^2 Q^2/(36h^2)\big)}, \tag{3.11}$$

where the constants P and Q are defined by

$$P = \left(\frac{48\cos(\theta) + 3\cos(2\theta) - 51}{11 + 4\cos(\theta)}\right), \quad Q = \left(\frac{28\sin(\theta) + \sin(2\theta)}{3 + 2\cos(\theta)}\right). \tag{3.12}$$

Proof. The stability of the Compact6 method holds if

$$|\mathcal{L}(\theta)|^2 \leq (1 + C\tau)^2 \cong 1 + 2C\tau, \tag{3.13}$$

where

$$C = \Re\frac{\gamma P/(2h^2) - i\alpha Q/(6h)}{1 - \delta P/(2h^2)}.$$

Using Eq. (3.10) and the notation defined in (3.12), we obtain

$$\frac{\gamma^2\tau^2 P^2}{4h^4} + 2\left(1 - \frac{\delta P}{2h^2}\right)\frac{\gamma\tau P}{2h^2} + \frac{\alpha^2\tau^2 Q^2}{36h^2} \leq 2C\tau\left(1 - \frac{\delta P}{2h^2}\right)^2. \tag{3.14}$$

Simplifying the above estimate results in (3.11).   □

Remark 3.1. By setting $\gamma = \delta = 0$ in Eq. (3.10), we derive the expression

$$|\mathcal{L}(\theta)|^2 = 1 + \frac{\alpha^2\tau^2}{36h^2}\left(\frac{28\sin(\theta) + \sin(2\theta)}{3 + 2\cos(\theta)}\right)^2 > 1, \quad \theta \neq l\pi, \quad l \in \mathbb{Z}^+. \tag{3.15}$$

This indicates that the Compact6 method is unconditionally unstable when $C = 0$.

3.1. Nonlinear stability analysis

The von Neumann method is a common tool for analyzing L^2-stability, but it is primarily applicable to linear schemes. Its application to nonlinear problems is generally limited. For nonlinear equations, stability can sometimes be analyzed using energy estimates, or in specific scenarios, one may consider L^∞-stability instead. For instance, L^∞-stability has been established for the Burgers-Fisher equation using cubic B-spline quasi-interpolation methods [42]. However, in the context of Sobolev-type equations, the presence of the dispersive term u_{xxt} makes the stability analysis challenging using these standard approaches [20].

An approach to investigate the L^2-stability of Sobolev-type equations with g = 0 is through a linearization process [35]. For example, consider the equation

$$u_t + f(u)_x - \gamma u_{xx} - \delta u_{xxt} = 0. \tag{3.16}$$

Assume a smooth solution u exists for some small interval $[t, t+\tau]$ within $(0, T)$. To approximate $u(x, t + \tau)$, we expand it using a Taylor series and ignore higher-order terms, yielding

$$u(x, t + \tau) \approx u(x, t) + \tau v(x, t), \tag{3.17}$$

where $v = u_t$. Expand $f(u)$ using Taylor series around the known solution $u(x, t)$ as

$$f(u)\Big|_{(x,t+\tau)} \approx f(u) + f'(u)\Delta u + \frac{1}{2}f''(u)(\Delta u)^2 + \cdots\Big|_{(x,t)}, \tag{3.18}$$

where $\Delta u \approx \tau\,v(x, t)$. For simplicity, higher-order terms $((\Delta u)^2, (\Delta u)^3, \cdots)$ are neglected, as they are small. Thus,

$$f(u)\Big|_{(x,t+\tau)} \approx f(u) + f'(u)\big(\tau v(x, t)\big). \tag{3.19}$$

Differentiate $f(u)$ with respect to x and using the Taylor expansion we get

$$f(u)_x\Big|_{(x,t+\tau)} \approx \frac{\partial}{\partial x}\big(f(u) + f'(u)\big(\tau v(x,t)\big)\big)$$

$$= f'(u)u_x + \tau\big(f'(u)v_x + f''(u)u_x v(x,t)\big). \tag{3.20}$$

Substituting Eqs. (3.17) and (3.20) into the governing equation and neglecting higher-order terms in τ, we get

$$v_t + f'(u)v_x - \gamma v_{xx} - \delta v_{xxt} + f''(u)u_x v(x,t) = 0. \tag{3.21}$$

By assuming that the solution u at time level t is known, the above equation can be analyzed for L^2-stability using the von Neumann approach, as described in Section 3.

4. Numerical Results

In this section, the performance of the sixth-order compact scheme is evaluated using several 1D and 2D numerical examples. Forward Euler is employed for time integration, with the time step chosen as $\tau = h^6$. Additionally, we compare the performance of our scheme with the cubic B-spline quasi-interpolation (CBSQI) and the improved cubic B-spline quasi-interpolation (ICBSQI) methods proposed in [20], where a fixed time step of $\tau = 10^{-4}$ is used.

Example 4.1 (Advection Free Flow). Consider the 1D linear Sobolev-type equation

$$u_t = u_{xx} + u_{xxt}, \quad (x,t) \in [0,30] \times [0,T] \tag{4.1}$$

with the initial condition $u(x,0) = \sin(x)$, for $x \in [0,30]$. The exact solution for this equation is given by $u(x,t) = e^{-t/2}\sin(x)$ over the domain $(x,t) \in [0,30] \times [0,T]$. For this initial value problem, we apply the Compact6 method, implementing boundary corrections as described in Section 2 using the exact solution for boundary terms. The numerical solution is computed at $T = 1$ over the spatial domain $[0,30]$. In Table 4.1, the L^∞, L^1, and L^2 errors and the convergence rates of the method are presented. As shown, the Compact6 method demonstrates numerical convergence to the exact solution at a rate of six, aligning well with theoretical results from Theorem 2.1. The numerical solutions and absolute error for $N = 150$ at time $T = 1$ is depicted in Fig. 4.1. Table 4.2 presents the error analysis and order of convergence at the final time $T = 1$, using a fixed spatial resolution of $N = 300$. The table reports numerical errors in the L^∞, L^1, and L^2 norms for decreasing time step sizes $\tau = 10^{-1}, 10^{-2}, 10^{-3}, 10^{-4}, 10^{-5}$. As shown in the table, the numerical scheme exhibits approximately first-order convergence in time across all norms, confirming the expected temporal accuracy of the method. Furthermore, Fig. 4.2 compares the L^∞ errors of the CBSQI, ICBSQI, and Compact6 schemes in $T = 1$ with $\tau = 0.0001$, indicating that the Compact6 scheme yields significantly smaller errors than the other two schemes.

A numerical verification of the exponential decay in the solution, as per Theorem 3.1, is conducted over the domain $[0, 2\pi]$ divided into 50 grid points. The graph in Fig. 4.3(i) illustrates the decay of the solution over time, and Fig. 4.3(ii) compares the left and right sides of estimate (3.8). This comparison shows that the numerical solution's magnitude remains within the bounds given by the right-hand side of the estimate, confirming exponential decay with respect to time.

Table 4.1: Errors and spatial order of convergence for Example 4.1.

N	L^∞-error	Rate	L^1-error	Rate	L^2-error	Rate
40	1.9599e-02	-	1.0490e-02	-	1.0883e-02	-
80	2.7099e-04	6.1764	1.4551e-04	6.1716	1.5698e-04	6.1154
160	3.9937e-06	6.0844	2.1853e-06	6.0572	2.3905e-06	6.0371
320	6.0537e-08	6.0438	3.3416e-08	6.0312	3.6895e-08	6.0177

Table 4.2: Errors and temporal order of convergence for Example 4.1 at $T = 1$ and $N = 300$.

τ	L^∞-error	Rate	L^1-error	Rate	L^2-error	Rate
1e-01	8.9386e-03	-	4.9551e-03	-	5.4720e-03	-
1e-02	8.7621e-04	1.0087	4.8405e-04	1.0102	5.3438e-04	1.0103
1e-03	8.7450e-05	1.0009	4.8294e-05	1.0010	5.3314e-05	1.0010
1e-04	8.7434e-06	1.0001	4.8283e-06	1.0001	5.3302e-06	1.0001
1e-05	8.7443e-07	1.0000	4.8285e-07	1.0000	5.3302e-07	1.0000

(i) Absolute error distribution   (ii) Numerical vs. exact solution
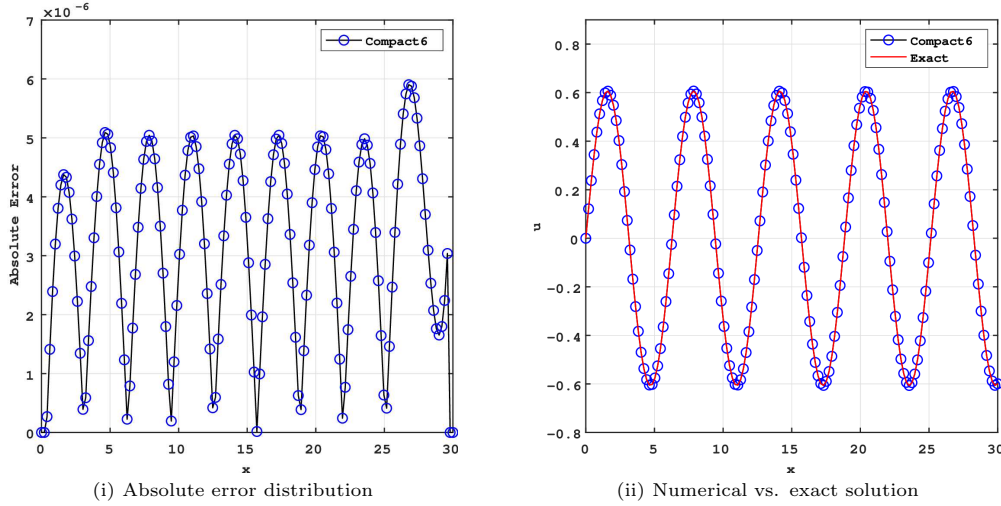
Fig. 4.1. (i) Absolute error distribution for the Compact6 method in Example 4.1 at $T = 1$. (ii) Comparison of the numerical solution from the Compact6 method (o symbols) with the exact solution (solid line) at $T = 1$.

Next, we examine the time-step constraints for stability in the Compact6 method. The stability limit based on (3.11) becomes $\tau \leq 2(1 + 7h^2/48)$. To validate this numerically, we run an experiment over the domain $[0, \pi]$ discretized into 100 intervals. In this setup, the stability bound allows $\tau = 2.00115$. The solutions obtained using the proposed method at $T = 1000$ are illustrated in Fig. 4.4. Due to the exponential time decay of the solution, the exact solution approaches zero at this large time. Fig. 4.4(a) shows the solutions with $\tau = 2$, where stability, as predicted by the stability estimates, is confirmed. Although the numerical solution deviates from the exact solution, it is bounded within 10^{-4}. By extending the time interval up to $T = 10,000$, Fig. 4.4(c) shows that the solutions remain bounded within 10^{-4}. In contrast,
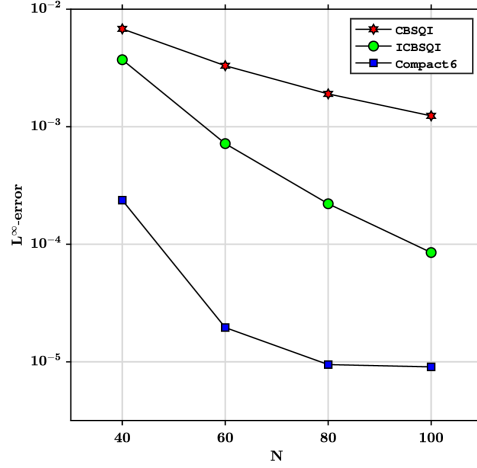
Fig. 4.2. Comparison of CBSQI, ICBSQI and Compact6 schemes in terms of L^∞ errors (in log10 scale) for Example 4.1 at $T = 1$ and $\tau = 0.0001$.

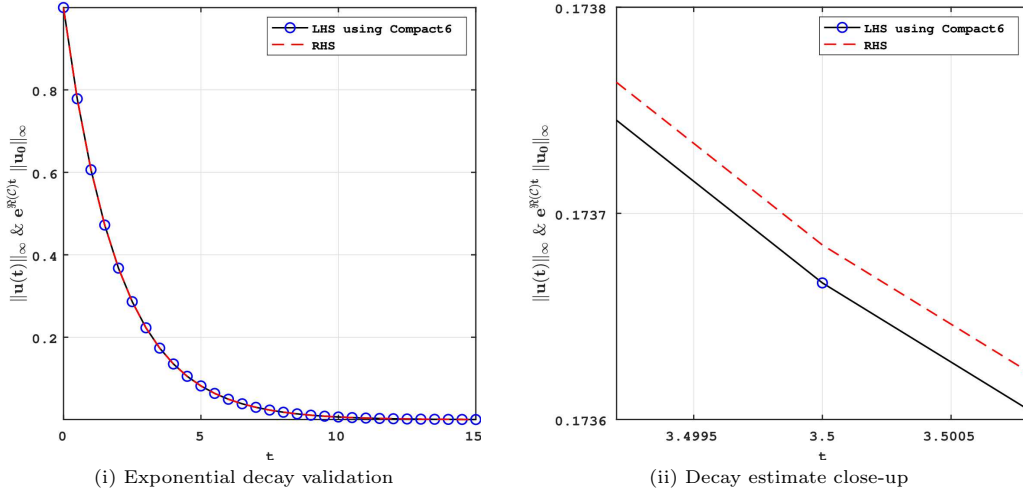(i) Exponential decay validation

(ii) Decay estimate close-up

Fig. 4.3. (i) Numerical validation of the exponential decay from Theorem 3.1 using the Compact6 method. (ii) Zoom around $t = 3.5$ showing the decay estimate (3.8). -o- line: left-hand side of (3.8), dashed line: right-hand side.

taking $\tau = 2.1$, just slightly beyond the stability bound, leads to solution blow-up, as seen in Figs. 4.4(b) and 4.4(d), where the maximum solution value increases to 10^{16} and reaches 10^{193} by $T = 10,000$.

Example 4.2 (Advection Free Flow). We consider the two-dimensional linear Sobolev-type equation [27] with vanishing source term

$$u_t = u_{xx} + u_{yy} + u_{xxt} + u_{yyt}, \quad (x, y, t) \in [0, 30] \times [0, 30] \times [0, T] \tag{4.2}$$

with initial condition $u(x, y, 0) = \sin(x)\sin(y)$. The exact solution is given by

$$u(x, y, t) = e^{-\frac{2t}{3}} \sin(x)\sin(y)$$

(a) Stable solution, $\tau = 2$, $T = 1000$

(b) Unstable solution, $\tau = 2.1$, $T = 1000$

(c) Stable solution, $\tau = 2$, $T = 10,000$

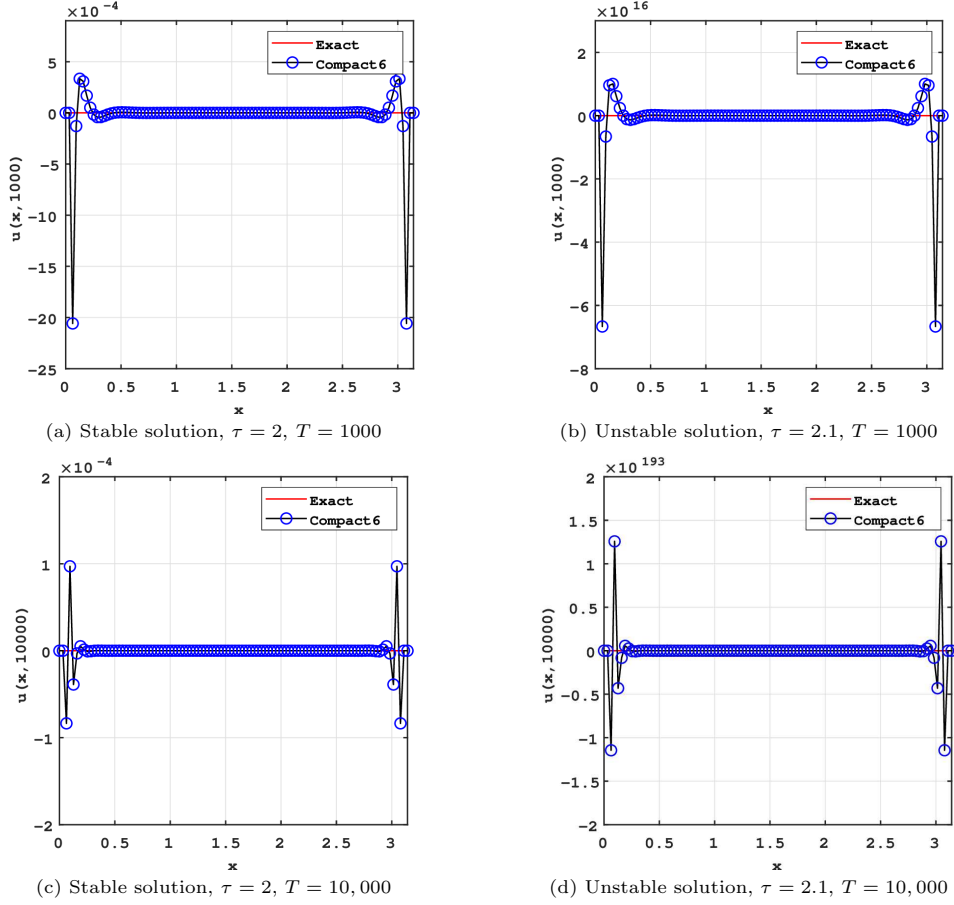(d) Unstable solution, $\tau = 2.1$, $T = 10,000$

Fig. 4.4. Numerical solutions obtained using the Compact6 method for Example 4.1 with $N = 100$: (a) $\tau = 2$ and (b) $\tau = 2.1$ at $T = 1000$, and (c) $\tau = 2$ and (d) $\tau = 2.1$ at $T = 10,000$.

in the same domain. The numerical results at $T = 1$ over the spatial region $[0, 30] \times [0, 30]$ are summarized in Table 4.3, showing L^∞, L^1, and L^2 errors along with the observed convergence rates. The results confirm that the Compact6 method attains sixth-order accuracy. Fig. 4.5 shows the numerical solution at $T = 1$. Fig. 4.5(i) presents the surface plot of the solution, while Fig. 4.5(ii) displays the corresponding contour plot. Both plots highlight the accuracy and resolution of the computed solution on a 320×320 grid.

Table 4.3: Errors and spatial order of convergence for Example 4.2 (Here $\tau = h^6$).

$N_x \times N_y$	L^∞-error	Rate	L^1-error	Rate	L^2-error	Rate
40×40	9.0298e-02	-	3.2364e-02	-	3.9275e-02	-
80×80	1.2381e-03	6.1885	4.2315e-04	6.2571	5.2048e-04	6.2376
160×160	2.6617e-05	5.5396	6.3855e-06	6.0502	7.8688e-06	6.0476
320×320	4.4120e-07	5.9148	9.7715e-08	6.0301	1.2091e-07	6.0241
640×640	6.9475e-09	5.9888	1.5097e-09	6.0163	1.8731e-09	6.0124
1280×1280	1.0840e-10	6.0020	2.3448e-11	6.0086	2.9140e-11	6.0063

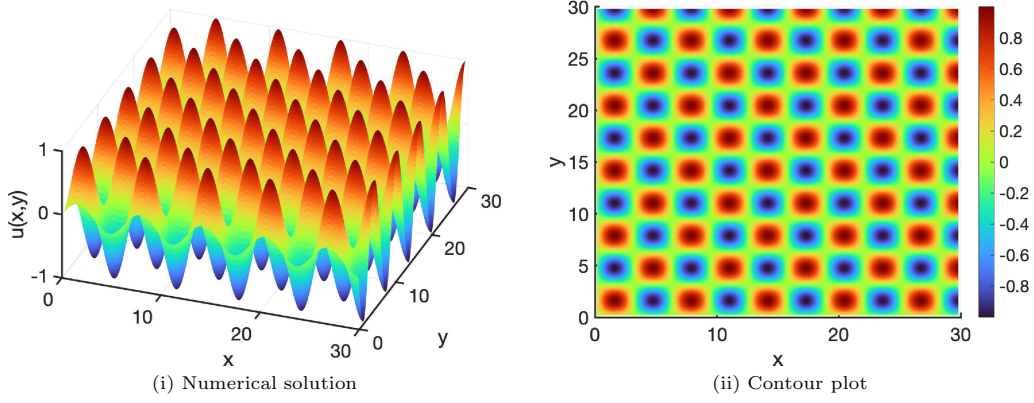(i) Numerical solution   (ii) Contour plot

Fig. 4.5. Numerical solution and corresponding contour plot obtained using the Compact6 scheme Example 4.2 at final time $T = 1$, with a grid resolution of $N_x \times N_y = 320 \times 320$.

Example 4.3 (Advection-Diffusion Flow). Consider the linear Sobolev-type equation

$$u_t + u_x = u_{xx} + u_{xxt}, \quad (x, t) \in [0, 30] \times [0, 1], \tag{4.3}$$

with the initial condition $u(x, 0) = \sin(x)$. The exact solution is given by

$$u(x, t) = e^{-\frac{t}{2}} \sin\left(x - \frac{t}{2}\right).$$

Implementing the Compact6 method with boundary correction, we use the exact solution to the boundary terms, following the approach outlined in the previous example. In Table 4.4, we report the L^∞, L^1, and L^2 errors, which indicate that the method achieves nearly sixth-order convergence. Table 4.5 displays the temporal error and convergence results at the final time $T = 1$, using a fixed spatial discretization of $N = 300$. The numerical scheme demonstrates clear first-order accuracy in time across all norms, validating its temporal convergence behavior. Additionally, the comparative analysis in Fig. 4.7 highlights the L^∞ errors of CBSQI, ICBSQI, and Compact6 schemes for different spatial resolutions with $\tau = 10^{-4}$. Among these, the Compact6 method consistently outperforms the others, yielding significantly smaller errors and showcasing its superior accuracy and robustness on uniform grids.

We then examine linear stability under the conditions specified by Eq. (3.11), where the stability criterion for the Compact6 method is

$$\tau \leq \frac{2(1 + 7h^2/48)}{1 + 507291h^2/9000000}.$$

Table 4.4: Errors and spatial order of convergence for Example 4.3.

N	L^∞-error	Rate	L^1-error	Rate	L^2-error	Rate
40	4.0010e-02	-	2.0771e-02	-	2.2165e-02	-
80	5.6453e-04	6.1472	2.8795e-04	6.1726	3.1281e-04	6.1468
160	8.2482e-06	6.0968	4.2936e-06	6.0675	4.7370e-06	6.0452
320	1.2505e-07	6.0435	6.5461e-08	6.0354	7.2949e-08	6.0209

Table 4.5: Errors and temporal order of convergence for Example 4.3 at $T = 1$ and $N = 300$.

τ	L^∞-error	Rate	L^1-error	Rate	L^2-error	Rate
1e-01	1.8553e-02	-	9.7956e-03	-	1.0902e-02	-
1e-02	1.8173e-03	1.0090	9.5157e-04	1.0126	1.0590e-03	1.0126
1e-03	1.8135e-04	1.0009	9.4883e-05	1.0013	1.0560e-04	1.0012
1e-04	1.8131e-05	1.0001	9.4855e-06	1.0001	1.0556e-05	1.0001
1e-05	1.8128e-06	1.0001	9.4836e-07	1.0001	1.0555e-06	1.0001

For $h = 0.0314$ and a computational interval of $[0, \pi]$, this yields an approximate stability threshold of 2. As observed in prior examples, our numerical tests support this threshold as optimal as shown in Fig. 4.6.

(i) Stable solution, $\tau = 2$ (ii) Unstable solution, $\tau = 2.1$
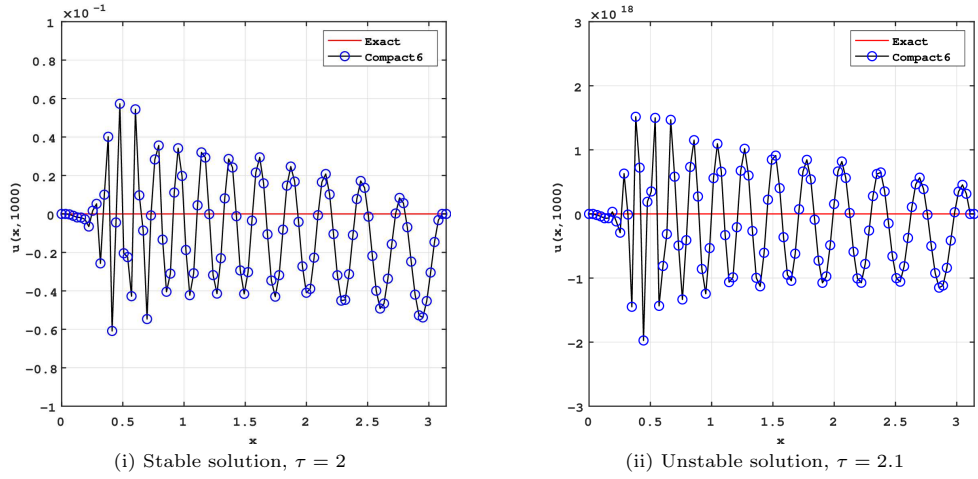
Fig. 4.6. Numerical solutions using the Compact6 method for Example 4.3 at $T = 1000$ with $N = 100$: (i) $\tau = 2$, (ii) $\tau = 2.1$.

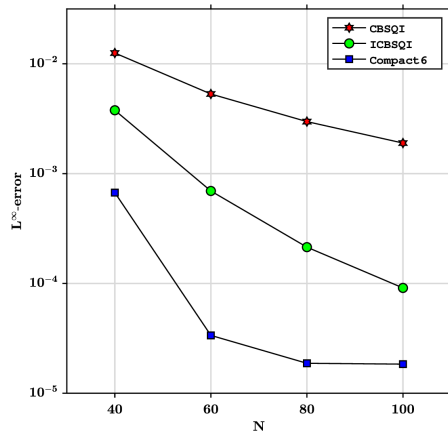Fig. 4.7. Comparison of CBSQI, ICBSQI and Compact6 schemes in terms of L^∞ errors (in log 10 scale) for Example 4.3 at $T = 1$ and $\tau = 0.0001$.

Example 4.4 (Advection-diffusion Flow). We extend the study to two dimensions by considering the 2D linear Sobolev-type equation

$$u_t + u_x + u_y = u_{xx} + u_{yy} + u_{xxt} + u_{yyt}, \quad (x, y, t) \in [0, 30] \times [0, 30] \times [0, 1], \qquad (4.4)$$

subject to the initial condition $u(x, y, 0) = \sin(x) \sin(y)$. The exact solution is given by

$$u(x, y, t) = e^{-\frac{2t}{3}} \sin\left(x - \frac{t}{3}\right) \sin\left(y - \frac{t}{3}\right).$$

The Compact6 method is employed to compute the solution, with boundary corrections extended from the 1D formulation. Table 4.6 presents the L^∞, L^1, and L^2 error norms, demonstrating that the scheme maintains nearly sixth-order accuracy in two dimensions as well.

We proceed by applying the Compact6 method to examine certain nonlinear Sobolev-type equations, specifically focusing on two cases: the EW equation and the BBMB equation. The EW equation is an advection-only model, neglecting any dissipation effects, while the BBMB equation incorporates advection, diffusion, and dispersion processes.

Table 4.6: Errors and spatial order of convergence for Example 4.4 (Here $\tau = h^6$).

$N_x \times N_y$	L^∞-error	Rate	L^1-error	Rate	L^2-error	Rate
40×40	9.4893e-02	-	3.9219e-02	-	4.7519e-02	-
80×80	2.3417e-03	5.3407	5.3359e-04	6.1997	6.4883e-04	6.1945
160×160	3.5648e-05	6.0376	8.1059e-06	6.0406	9.9268e-06	6.0304
320×320	5.3646e-07	6.0542	1.2449e-07	6.0248	1.5323e-07	6.0176
640×640	8.1970e-09	6.0322	1.9265e-09	6.0139	2.3783e-09	6.0096
1280×1280	1.2659e-10	6.0168	2.9949e-11	6.0073	3.7032e-11	6.0050

4.1. Equal width equation

Similar to the RLW equation, the EW equation is characterized by three conserved quantities, representing mass, momentum, and energy, respectively. Olver [26] demonstrated that the EW equation can be reformulated in a conservative form $\eta_t + \chi_x = 0$ in only three distinct, non-trivial ways, where $\eta = \eta(u, u_x)$ and $\chi = \chi(u, u_t, u_{xt})$. These invariants are given by

$$\mathfrak{I}_1 = \int_{-\infty}^{\infty} u\,dx, \quad \mathfrak{I}_2 = \int_{-\infty}^{\infty} \left(u^2 + \delta u_x^2\right) dx, \quad \mathfrak{I}_3 = \int_{-\infty}^{\infty} u^3 dx. \qquad (4.5)$$

To approximate these integrals, we utilized the composite Simpson's rule. This section investigates four test cases to assess the effectiveness of the proposed numerical method: solitary wave solutions, interactions between two solitary waves, interactions of three solitary waves, and the undular bore phenomenon.

Example 4.5 (Propagation of a Single Solitary Wave). Consider the equal width equation (1.3) with the initial condition

$$u(x, 0) = 3c \operatorname{sech}^2\left(k(x - x_0)\right), \quad x \in [0, 30] \qquad (4.6)$$

along with the homogeneous Dirichlet boundary conditions

$$u(0, t) = 0, \quad u(30, t) = 0. \qquad (4.7)$$

The exact solution is given by

$$u(x,t) = 3c \operatorname{sech}^2\big(k(x - x_0 - ct)\big). \tag{4.8}$$

This solution represents the movement of a solitary wave with an amplitude of $3c$ and a width of k, initially centered at $x = x_0$, where $k = \sqrt{1/(4\delta)}$ and c denotes the wave speed. Here, $\delta = 1, c = 0.03, x_0 = 10$. Table 4.7 provides a summary of the L^∞-error, L^1-error, L^2-error, and the order of convergence for considered scheme at the final time $T = 200$. Fig. 4.8(a) illustrates the absolute error, while Fig. 4.8(b) compares the numerical solution obtained using the Compact6 method with the exact solution at times $T = 0$ and $T = 200$. Fig. 4.9 provides a comparative study of the L^∞ errors at final time $T = 200$, with a fixed time step size

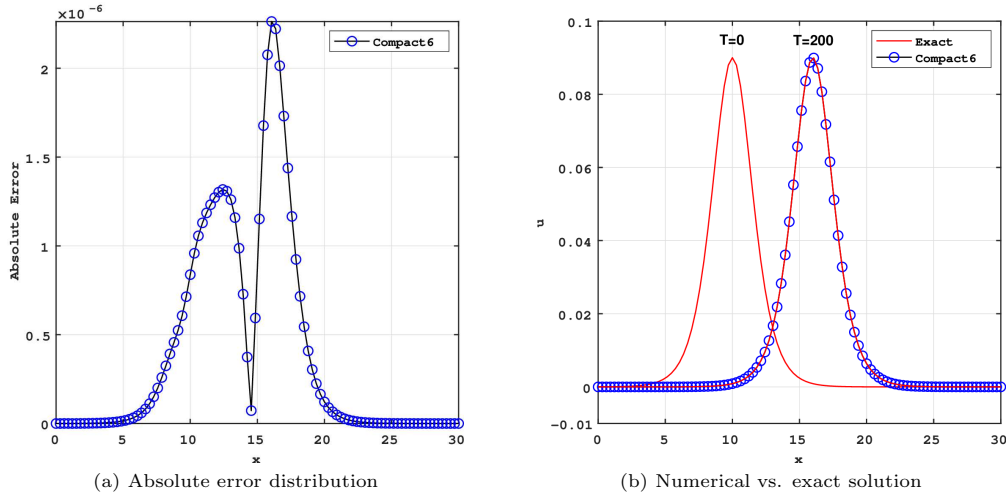(a) Absolute error distribution   (b) Numerical vs. exact solution

Fig. 4.8. (a) Absolute error distribution for the Compact6 method in Example 4.5 at $T = 200$. (b) Comparison of the numerical solution from the Compact6 method (o symbols) with the exact solution (solid line) at $T = 200$ with $N = 100$.
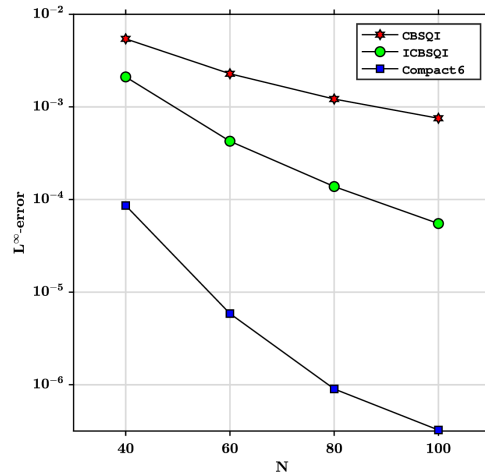

Fig. 4.9. Comparison of CBSQI, ICBSQI and Compact6 schemes in terms of L^∞ errors (in log10 scale) for Example 4.5 at $T = 200$ and $\tau = 0.0001$.

$\tau = 10^{-4}$. The results clearly indicate that the Compact6 scheme achieves significantly lower errors compared to the CBSQI and ICBSQI methods across all tested spatial resolutions. This demonstrates the high accuracy and stability of the Compact6 approach, especially for long-time integration.

For solitary wave solutions (4.8), each form of χ satisfies

$$\chi \;\to\; 0 \quad \text{as} \quad x \;\to\; \pm\infty, \tag{4.9}$$

implying that the integrals

$$\mathfrak{I}_j = \int_{-\infty}^{\infty} \eta_j dx, \quad j = 1, 2, 3, \tag{4.10}$$

remain invariant over time. Given that the solution in this example is smooth, it must satisfy all three conservation laws. Thus, the invariants $\mathfrak{I}_1, \mathfrak{I}_2$, and $\mathfrak{I}_3$ remain constant for the solitary wave solution, serving as a benchmark for evaluating the conservation properties of numerical methods. To validate this property, we conducted numerical experiments, limiting the domain of integration to $[0, 30]$ due to the decay of the solitary wave solution outside this interval. The analytical expressions for these invariants, provided in [14], are given by

$$\mathfrak{I}_1 = \frac{6c}{k}, \quad \mathfrak{I}_2 = \frac{12c^2}{k} + \frac{48kc^2\delta}{5}, \quad \mathfrak{I}_3 = \frac{144c^3}{5k}. \tag{4.11}$$

For $c = 0.03$, the exact values of $\mathfrak{I}_1, \mathfrak{I}_2$, and $\mathfrak{I}_3$ are $0.36, 0.02592$, and 1.5552×10^{-3}, respectively. Table 4.8 summarizes the numerical values obtained for these invariants and their respective percentage errors, showing that $\mathfrak{I}_1, \mathfrak{I}_2$, and $\mathfrak{I}_3$ remain effectively constant throughout the simulation. At $t = 25$, the relative changes in the invariants $\mathfrak{I}_1, \mathfrak{I}_2$, and $\mathfrak{I}_3$ for this method are $2.3237e\text{-}03\%, 1.4909e\text{-}04\%$, and $2.3542e\text{-}04\%$, respectively. The close agreement between the numerical results and the analytical values supports the time invariance of these integrals, validating the conservation properties of the method used.

Table 4.7: Errors and spatial order of convergence for Example 4.5.

N	L^∞-error	Rate	L^1-error	Rate	L^2-error	Rate
40	5.9911e-04	-	1.1793e-04	-	1.8701e-04	-
80	8.6472e-06	6.1144	1.6380e-06	6.1698	2.7540e-06	6.0855
160	1.3224e-07	6.0310	2.4203e-08	6.0807	4.1772e-08	6.0428

Table 4.8: Invariants for a single solitary wave in Example 4.5 over the domain $\Omega = [0, 30]$ with $N = 120$.

Time	$\mathfrak{I}_1$	% Error of $\mathfrak{I}_1$	$\mathfrak{I}_2$	% Error of $\mathfrak{I}_2$	$\mathfrak{I}_3$	% Error of $\mathfrak{I}_3$
5	3.5998e-01	4.2334e-03	2.5920e-02	2.6234e-05	1.5552e-03	4.7084e-05
10	3.5999e-01	3.6438e-03	2.5920e-02	5.6620e-05	1.5552e-03	9.4169e-05
15	3.5999e-01	3.1363e-03	2.5920e-02	8.7267e-05	1.5552e-03	1.4125e-04
20	3.5999e-01	2.6996e-03	2.5920e-02	1.1811e-04	1.5552e-03	1.8834e-04
25	3.5999e-01	2.3237e-03	2.5920e-02	1.4909e-04	1.5552e-03	2.3542e-04

Example 4.6 (Interaction of Two Solitary Waves). To analyze the interaction of two solitary waves, we consider Eq. (1.3) with the following initial and boundary conditions:

$$u(x,0) = 3\sum_{j=1}^{2} c_j \operatorname{sech}^2\big(k_j(x - x_j)\big), \quad x \in [0, 70],$$

$$u(0,t) = 0, \quad u(70,t) = 0.$$

$$(4.12)$$

For the numerical simulations, the parameters are set as $k_1 = k_2 = 0.5, \delta = 1, c_1 = 0.2, c_2 = 0.4,$ $x_1 = 10, x_2 = 25$. The analytical values [30] of the three invariants in (4.5) can be calculated as follows:

$$\mathfrak{I}_1 = 12(c_1 + c_2) = 7.2, \quad \mathfrak{I}_2 = 28.8\big(c_1^2 + c_2^2\big) = 5.76, \quad \mathfrak{I}_3 = 57.6\big(c_1^3 + c_2^3\big) = 4.1472. \quad (4.13)$$

Table 4.9 presents the invariant values calculated at time points representing the pre-interaction phase ($T = 10$), interaction stages ($T = 45, 55$, and 65), and post-interaction phase ($T = 100$). The relative changes in the invariants $\mathfrak{I}_1, \mathfrak{I}_2$, and $\mathfrak{I}_3$ at $t = 25$ for the current method are $3.3634\text{e-}03\%, 5.5535\text{e-}02\%$, and $8.9002\text{e-}02\%$, respectively. The solution profiles at various time instances are shown in Fig. 4.10. These graphs illustrate that, over time, the wave with the larger amplitude overtakes and moves ahead of the smaller amplitude wave.

Table 4.9: Invariants for the interaction of two solitary waves in Example 4.6 over the domain $\Omega = [0, 70]$ with $N = 300$.

Time	$\mathfrak{I}_1$	% Error of $\mathfrak{I}_1$	$\mathfrak{I}_2$	% Error of $\mathfrak{I}_2$	$\mathfrak{I}_3$	% Error of $\mathfrak{I}_3$
10	7.2002	3.2146e-03	5.7604	6.5176e-03	4.1476	1.0761e-02
45	7.2002	3.3619e-03	5.7616	2.8086e-02	4.1491	4.5583e-02
55	7.2002	3.3632e-03	5.7619	3.2720e-02	4.1494	5.2814e-02
65	7.2002	3.3644e-03	5.7621	3.5805e-02	4.1496	5.7325e-02
100	7.2002	3.3634e-03	5.7632	5.5535e-02	4.1509	8.9002e-02

Example 4.7 (Interaction of Three Solitary Waves). The initial condition for Eq. (1.3) is defined as

$$u(x,0) = 3\sum_{j=1}^{3} c_j \operatorname{sech}^2\big(k_j(x - x_j)\big), \quad x \in [-10, 100], \quad (4.14)$$

which characterizes a combination of three solitary waves traveling in the same direction. We impose the boundary conditions $u(a,0) = 0$ and $u(b,0) = 0$, with $a = -10$ and $b = 100$. The time interval is taken as $t \in [0, 15]$, and we use $N = 600$ evenly spaced points across this spatial domain. For the parameters, we set $k_i = 0.5$ (for $i = 1, 2, 3$), $c_1 = 4.5, c_2 = 1.5, c_3 = 0.5$, and positions $x_1 = 10, x_2 = 25, x_3 = 35$. Calculated values for the three conserved quantities are listed in Table 4.10, showing that they closely match their theoretical values. Specifically, the invariants are given as follows:

$$\mathfrak{I}_1 = 12(c_1 + c_2 + c_3) = 78,$$
$$\mathfrak{I}_2 = 28.8\big(c_1^2 + c_2^2 + c_3^2\big) = 655.2, \quad (4.15)$$
$$\mathfrak{I}_3 = 57.6\big(c_1^3 + c_2^3 + c_3^3\big) = 5450.4.$$

The results confirm that the invariants are well-preserved. The interactions of the three solitary waves are depicted in Fig. 4.11.

(a) $T = 10$

(b) $T = 45$

(c) $T = 65$

(d) $T = 100$

(e) Wave simulation across various time
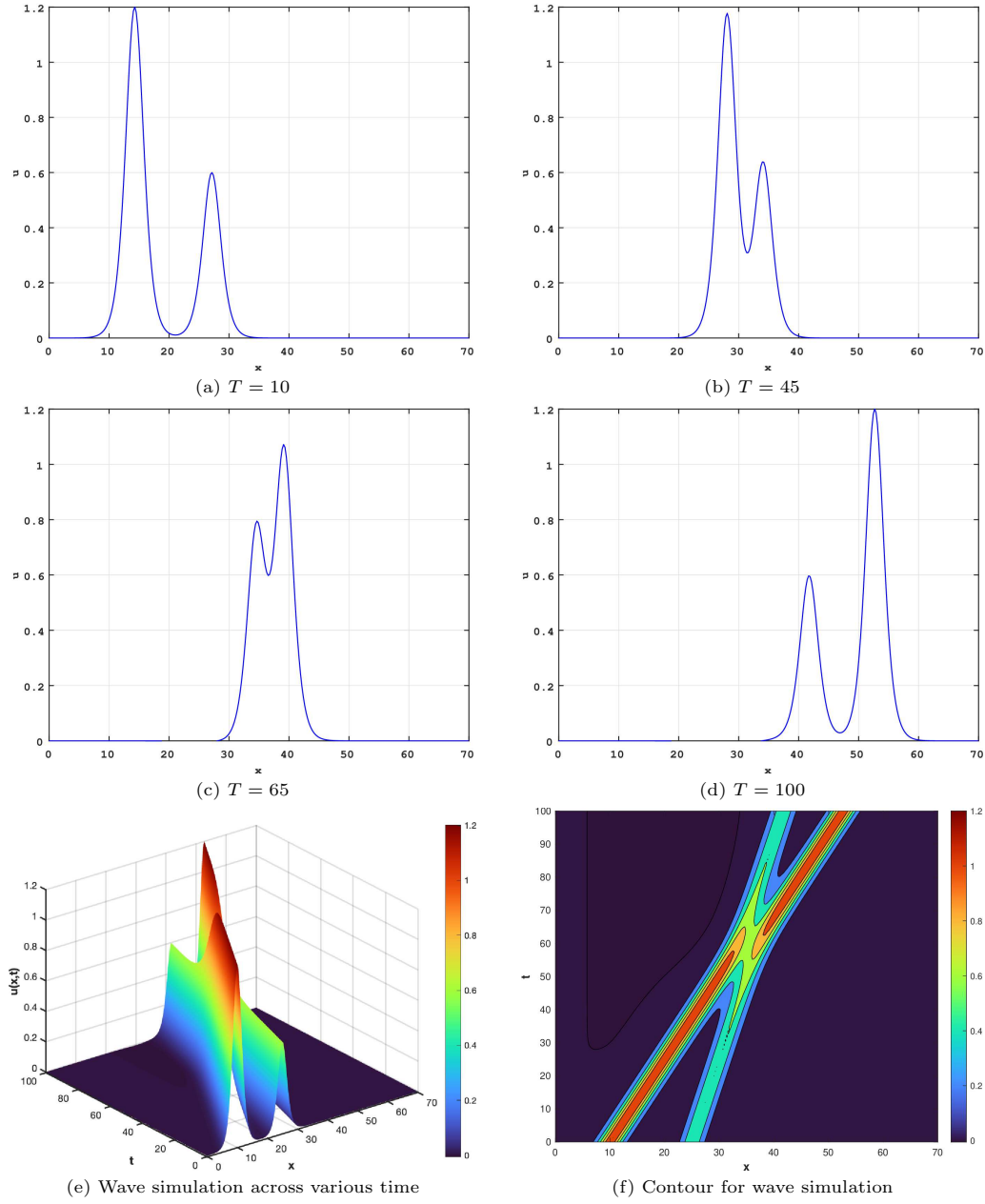
(f) Contour for wave simulation

Fig. 4.10. Numerical solution of EW equation with $N = 300$ and $0 \leq T \leq 100$ for Example 4.6.

Table 4.10: Invariants for the interaction of three solitary waves in Example 4.7 over the domain $\Omega = [-10, 100]$ with $N = 600$.

Time	$\mathfrak{I}_1$	% Error of $\mathfrak{I}_1$	$\mathfrak{I}_2$	% Error of $\mathfrak{I}_2$	$\mathfrak{I}_3$	% Error of $\mathfrak{I}_3$
1	78.0000	2.0158e-07	655.3505	2.2971e-02	5452.2761	3.4422e-02
5	78.0000	2.0545e-07	655.7636	8.6019e-02	5457.9016	1.3763e-01
10	78.0000	2.0545e-07	656.3525	1.7591e-01	5465.9593	2.8547e-01
15	78.0000	8.7733e-08	657.0034	2.7525e-01	5474.6982	4.4581e-01

(a) $T = 1$

(b) $T = 5$

(c) $T = 10$

(d) $T = 15$

(e) Wave simulation across various time
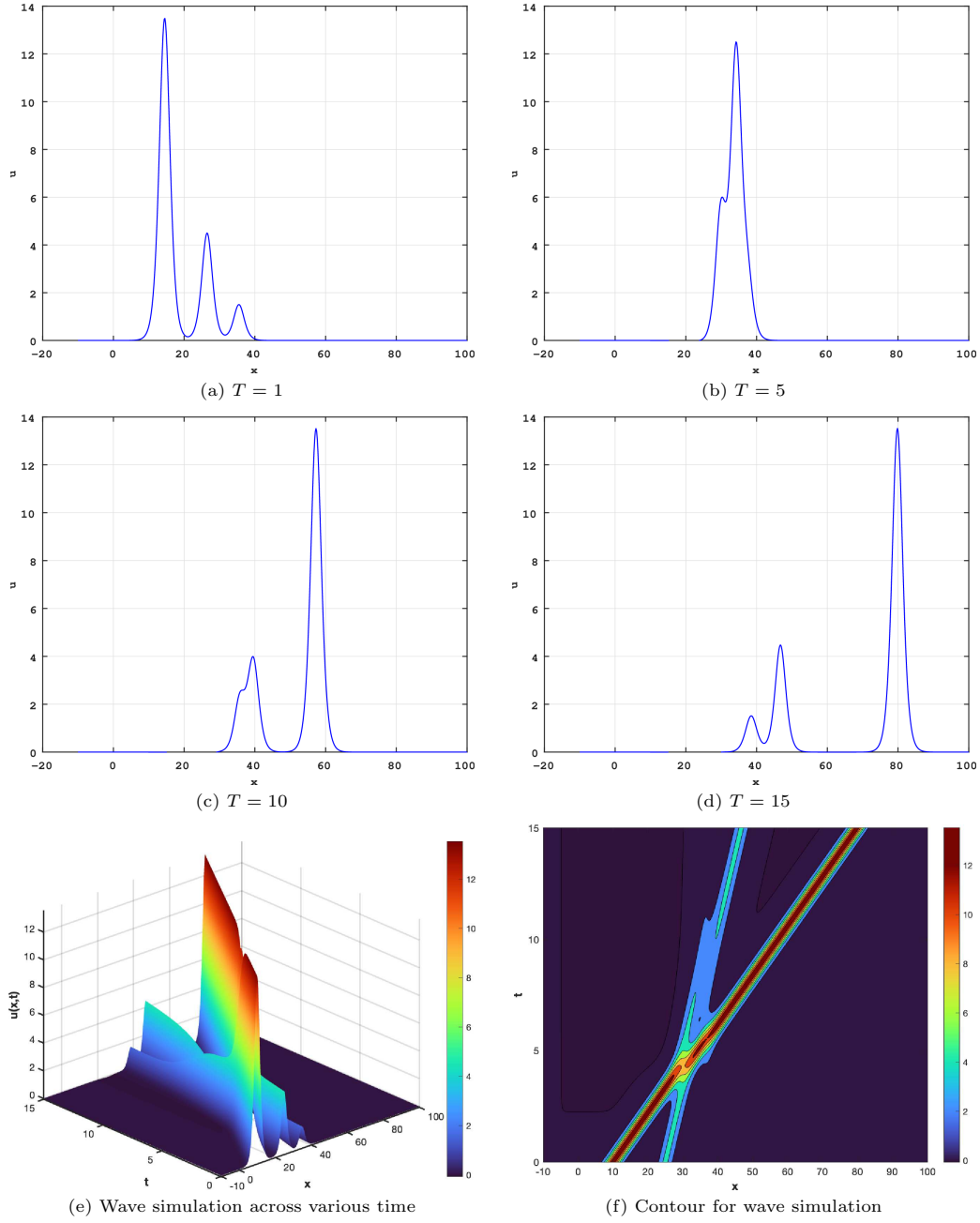

(f) Contour for wave simulation

Fig. 4.11. Numerical solution of EW equation with $N = 300$ and $0 \leq T \leq 15$ for Example 4.7.

Example 4.8 (Undular Bore). Next, the formation of an undular bore is examined using the following initial function, with the boundary condition:

$$u(x,0) = \frac{1}{2}u_0\left(1 - \tanh\left(\frac{x - x_c}{d}\right)\right), \tag{4.16}$$

$$u \rightarrow 0 \quad \text{as} \quad x \rightarrow \infty, \quad u \rightarrow u_0 \quad \text{as} \quad x \rightarrow -\infty. \tag{4.17}$$

Here, $u(x,0)$ indicates the elevation of the water surface above the equilibrium position at $t = 0$, the constants u_0, d, and x_c represent the magnitude of the water level change, the slope between shallow and deep water, and the center of the disturbance, respectively. In this case, we set $u_0 = 0.1, d = 5, x_c = 0$. The numerical solution is computed within the domain $-20 \leq x \leq 80$. As the wave moves forward, the nonlinear term uu_x in Eq. (1.3) causes a steepening effect, leading to an increase in u_x. This behavior is evident in the numerical results at $T = 70$, calculated with the Compact6 method, as illustrated in Fig. 4.12(a). When the dispersive term is absent, the wave forms a shock at the critical time $t^* = 100$, and a weak solution with shock discontinuity persists for $t > t^*$. However, with the inclusion of the dispersive term u_{xxt} in Eq. (1.3), the wave evolves into an undular bore, as seen in Fig. 4.12(b). These simulations demonstrate that the Compact6 method effectively captures the dispersive effects.

The integrals $\mathfrak{I}_1, \mathfrak{I}_2$, and $\mathfrak{I}_3$ defined in Eq. (4.5), are no longer constant because the fluxes χ do not meet the conditions outlined in Eq. (4.9). Table 4.11 shows the values of these integrals, along with the position and amplitude (equal to $\|u\|_\infty$) of the leading undulation at various time levels. The time-dependent variation of integrals $\mathfrak{I}_1, \mathfrak{I}_2$, and $\mathfrak{I}_3$ can be analytically computed and is expressed by

$$
\begin{aligned}
M_1 &= \frac{d\mathfrak{I}_1}{dt} = \frac{d}{dt} \int_{-\infty}^{\infty} u\,dx = \frac{1}{2}u_0^2 = 5 \times 10^{-3}, \\
M_2 &= \frac{d\mathfrak{I}_2}{dt} = \frac{d}{dt} \int_{-\infty}^{\infty} \left(u^2 + \delta u_x^2 \right) dx = \frac{2}{3}u_0^3 = 6.6667 \times 10^{-4}, \qquad (4.18)\\
M_3 &= \frac{d\mathfrak{I}_3}{dt} = \frac{d}{dt} \int_{-\infty}^{\infty} u^3\,dx = \frac{3}{4}u_0^4 = 7.5 \times 10^{-5}.
\end{aligned}
$$

The results obtained from the Compact6 method for the time rate of change of the integrals are in close agreement with the analytical values. The calculated values are $M_1 = 4.9994 \times 10^{-3}$, $M_2 = 6.6658 \times 10^{-4}$, and $M_3 = 7.4985 \times 10^{-5}$.

Example 4.9. Here, we examine the inhomogeneous BBMB equation (1.4), using the initial condition

$$
u(x,0) = u(x,0) = \text{sech}(x), \quad -10 < x < 10, \qquad (4.19)
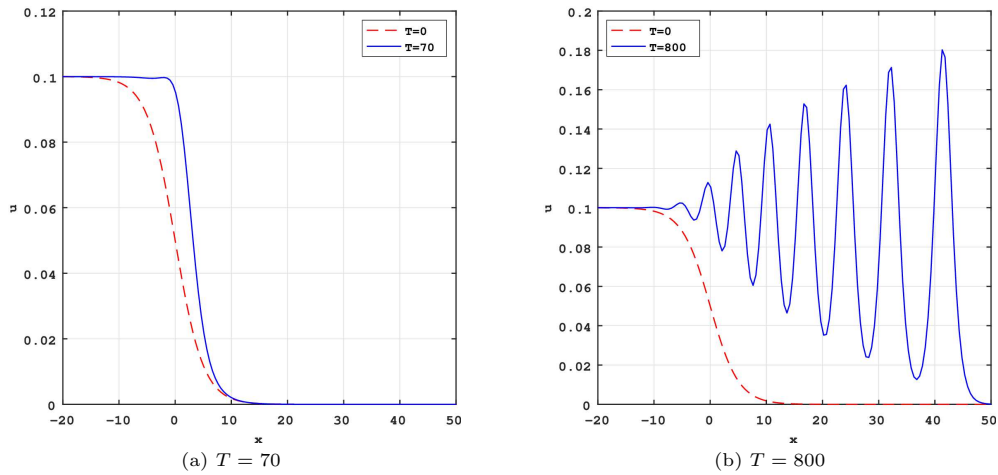$$

(a) $T = 70$ (b) $T = 800$

Fig. 4.12. Numerical solution of EW equation with $N = 200$ for Example 4.16.

Table 4.11: Development of an undular bore $\delta = 1, u_0 = 0.1, d = 5, -20 \le x \le 80, N = 200$: $\mathfrak{I}_1, \mathfrak{I}_2, \mathfrak{I}_3$ and the position x and amplitude $\|u\|_\infty$ of the leading undulation.

Time	$\mathfrak{I}_1$	$\mathfrak{I}_2$	$\mathfrak{I}_3$	x	$\|u\|_\infty$
150	2.749873	0.284106	0.027498	4.00	0.123733
200	2.999882	0.317460	0.031252	6.50	0.142425
300	3.499897	0.384223	0.038767	12.00	0.165481
400	3.999897	0.451066	0.046296	17.50	0.170815
600	4.999896	0.585010	0.061398	29.50	0.178813
800	5.999897	0.719309	0.076557	41.50	0.181478

and the boundary conditions

$$u(a,t) = \text{sech}(a-t), \quad u(b,t) = \text{sech}(b-t), \quad 0 < t < T. \tag{4.20}$$

The forcing term g is chosen as

$$\text{g}(x,t) = \left(1 - 6\tanh^3(x-t) - 2\tanh^2(x-t) - \left(\text{sech}(x-t) - 5\right)\tanh(x-t)\right)\text{sech}(x-t), \tag{4.21}$$

following the formulation proposed by Dehghan *et al.* [8], which yields the exact solution $u(x,t) = \text{sech}(x-t)$. Using the Compact6 method, we approximate the solution at $T = 1$ with the interval $[-10, 10]$ and the specified initial and boundary conditions. The error analysis, presented in Table 4.12, demonstrates the accuracy of our results in L^1, L^2, and L^∞ norms, showing that the method achieves sixth-order accuracy. Fig. 4.13 illustrates the comparison

Table 4.12: Errors and spatial order of convergence for Example 4.9.

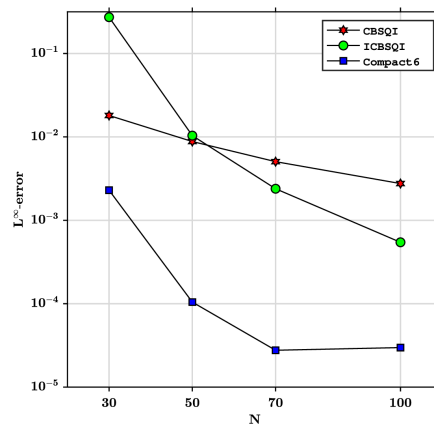| N	L^∞-error	Rate	L^1-error	Rate	L^2-error	Rate
40	5.0752e-03	-	8.3908e-04	-	1.4121e-03	-
80	7.7037e-05	6.0418	1.1634e-05	6.1724	2.0708e-05	6.0915
160	1.1704e-06	6.0404	1.7234e-07	6.0769	3.1358e-07	6.0452
320	1.7996e-08	6.0232	2.6243e-09	6.0372	4.8375e-09	6.0184

Fig. 4.13. Comparison of CBSQI, ICBSQI and Compact6 schemes in terms of L^∞ errors (in $\log 10$ scale) for Example 4.9 at $T = 1$ and $\tau = 0.0001$.

of L^∞ errors at the final time $T = 1$, using a fixed time step size $\tau = 10^{-4}$. The Compact6 scheme consistently yields lower errors than the CBSQI and ICBSQI methods, reinforcing its high precision and suitability for accurately solving the problem.

5. Conclusion

In this study, we developed a sixth-order compact finite difference scheme, Compact6, aimed at achieving high-accuracy numerical solutions for Sobolev-type equations. We began by outlining the Compact6 scheme for approximating both first and second-order derivatives, detailing the boundary treatments essential for practical implementation. The temporal derivatives are approximated using the explicit forward Euler difference method. The stability of the Compact6 method was rigorously analyzed in terms of L_2-stability, for the linear case. Using von Neumann stability analysis, we derived conditions under which the scheme remains stable and examined the amplification factor, $\mathcal{C}(\theta)$, to ensure its decay properties. To validate the accuracy and effectiveness of the Compact6 scheme, we conducted extensive numerical experiments. The tests included cases of 1D and 2D advection-free flow, advection-diffusion flow, and applications involving the equal width equation – such as single solitary wave propagation, interactions of two and three solitary waves, and the formation of undular bores. Additionally, tests were conducted on the Benjamin-Bona-Mahony-Burgers equation.

A comprehensive comparison of the L^∞, L^1, and L^2 error norms and the associated convergence rates demonstrates that the proposed Compact6 scheme achieves approximately first-order temporal accuracy when coupled with the forward Euler method. The numerical results also consistently show that Compact6 significantly outperforms the existing CBSQI and ICBSQI schemes in terms of accuracy across various test problems and spatial resolutions. This superiority is evident not only in short-time simulations but also in long-time integrations, thereby affirming the robustness, stability, and high precision of the Compact6 approach for solving a wide range of Sobolev-type equations.

References

[1] S. Abbasbandy and A. Shirzadi, The first integral method for modified Benjamin-Bona-Mahony equation, *Commun. Nonlinear Sci. Numer. Simul.*, **15**:7 (2010), 1759–1764.

[2] T. Achouri, N. Khiari, and K. Omrani, On the convergence of difference schemes for the Benjamin-Bona-Mahony (BBM) equation, *Appl. Math. Comput.*, **182**:2 (2006), 999–1005.

[3] B.S. Bahrami, H. Abdollahzadeh, I.M. Berijani, D.D. Ganji, and M. Abdollahzadeh, Exact travelling solutions for some nonlinear physical models by (G′/G)-expansion method, *Pramana*, **77** (2011), 263–275.

[4] G.I. Barenblatt, Iu.P. Zheltov, and I.N. Kochina, Basic concepts in the theory of seepage of homogeneous liquids in fissured rocks [strata], *J. Appl. Math. Mech.*, **24**:5 (1960), 1286–1303.

[5] M.S. Bruzón, Weak self-adjointness and conservation laws for a family of Benjamin-Bona-Mahony-Burgers equations, in: *Discontinuity and Complexity in Nonlinear Physical Systems. Nonlinear Systems and Complexity*, Vol. 6, Springer, (2013), 23–34.

[6] M.S. Bruzón and M.L. Gandarias, Conservation laws for a family of Benjamin-Bona-Mahony-Burgers equations, in: *Proceedings of the 2012 IEEE 4th International Conference on Nonlinear Science and Complexity (NSC)*, IEEE, (2012), 155–160.

[7] M.S. Bruzón, T.M. Garrido, and R. De la Rosa, Conservation laws and exact solutions of a Generalized Benjamin-Bona-Mahony-Burgers equation, *Chaos Solitons Fractals*, **89** (2016), 578–583.

[8] M. Dehghan, M. Abbaszadeh, and A. Mohebbi, The numerical solution of nonlinear high dimensional generalized Benjamin-Bona-Mahony-Burgers equation via the meshless method of radial basis functions, *Comput. Math. Appl.*, **68**:3 (2014), 212–237.

[9] A. Esen, A numerical solution of the equal width wave equation by a lumped Galerkin method, *Appl. Math. Comput.*, **168**:1 (2005), 270–282.

[10] R.E. Ewing, A coupled non-linear hyperbolic-Sobolev system, *Ann. Mat. Pura Appl.*, **114** (1977), 331–349.

[11] Z.Z. Ganji, D.D. Ganji, and H. Bararnia, Approximate general and explicit solutions of nonlinear BBMB equations by Exp-Function method, *Appl. Math. Model.*, **33**:4 (2009), 1836–1841.

[12] F. Gao, J. Cui, and G. Zhao, Weak Galerkin finite element methods for Sobolev equation, *J. Comput. Appl. Math.*, **317** (2017), 188–202.

[13] F. Gao and X. Wang, A modified weak Galerkin finite element method for Sobolev equation, *J. Comput. Math.*, **33** (2015), 307–322.

[14] L.R.T. Gardner, G.A. Gardner, F.A. Ayoub, and N.K. Amein, Simulations of the EW undular bore, *Commun. Numer. Methods Eng.*, **13**:7 (1997), 583–592.

[15] C.A. Gómez S., A.H. Salas, B.A. Frias, New periodic and soliton solutions for the Generalized BBM and Burgers-BBM equations, *Appl. Math. Comput.*, **217**:4 (2010), 1430–1434.

[16] C. Guo and S. Fang, Optimal decay rates of solutions for a multidimensional generalized Benjamin-Bona-Mahony equation, *Nonlinear Anal. Theory Methods Appl.*, **75**:7 (2012), 3385–3392.

[17] S. Hamdi, W.H. Enright, W.E. Schiesser, and J.J. Gottlieb, Exact solutions of the generalized equal width wave equation, in: *International Conference on Computational Science and Its Applications*, Springer, (2003), 725–734.

[18] S.R. Jena and A. Senapati, On numerical soliton and convergence analysis of Benjamin-Bona-Mahony-Burger equation via octic B-spline collocation, *Arab J. Basic Appl. Sci.*, **30**:1 (2023), 146–163.

[19] P. Joshi, M. Pathak, and J. Lin, Numerical study of generalized 2-D nonlinear Benjamin-Bona-Mahony-Burgers equation using modified cubic B-spline differential quadrature method, *Alexandria Eng. J.*, **67** (2023), 409–424.

[20] R. Kumar and S. Baskar, B-spline quasi-interpolation based numerical methods for some Sobolev type equations, *J. Comput. Appl. Math.*, **292** (2016), 41–66.

[21] R. Kumar, A. Choudhary, and S. Baskar, Modified cubic B-spline quasi-interpolation numerical scheme for hyperbolic conservation laws, *Appl. Anal.*, **99**:1 (2020), 158–179.

[22] S.K. Lele, Compact finite difference schemes with spectral-like resolution, *J. Comput. Phys.*, **103**:1 (1992), 16–42.

[23] R.J. LeVeque, *Finite Volume Methods for Hyperbolic Problems*, Cambridge University Press, 2002.

[24] P.J. Morrison, J.D. Meiss, and J.R. Cary, Scattering of regularized-long-wave solitary waves, *Physica D*, **11**:3 (1984), 324–336.

[25] M.A. Noor, K.I. Noor, A. Waheed, and E.A. Al-Said, Some new solitonary solutions of the modified Benjamin-Bona-Mahony equation, *Comput. Math. Appl.*, **62**:4 (2011), 2126–2131.

[26] P.J. Olver, Euler operators and conservation laws of the BBM equation, in: *Math. Proc. Cambridge Philos. Soc.*, **85**:1, (1979), 143–160.

[27] Ö. Oruç, A computational method based on Hermite wavelets for two-dimensional Sobolev and regularized long wave equations in fluids, *Numer. Methods Partial Differential Equations*, **34**:5 (2018), 1693–1715.

[28] D.H. Peregrine, Calculations of the development of an undular bore, *J. Fluid Mech.*, **25**:2 (1966),

321–330.

[29] X. Qinghua and C. Zhengzheng, Degenerate boundary layer solutions to the generalized Benjamin-Bona-Mahony-Burgers equation, *Acta Math. Sci.*, **32**:5 (2012), 1743–1758.

[30] K.R. Raslan, A computational method for the equal width equation, *Int. J. Comput. Math.*, **81**:1 (2004), 63–72.

[31] B. Saka, A finite element method for equal width equation, *Appl. Math. Comput.*, **175**:1 (2006), 730–747.

[32] L.V. Salian and R. Samala, Exponential approximation space reconstruction weighted essentially nonoscillatory scheme for dispersive partial differential equations, *Math. Methods Appl. Sci.*, **47**:4 (2024), 1823–1851.

[33] L.V. Salian, R. Samala, and D. Ghosh, A novel central compact finite-difference scheme for third derivatives with high spectral resolution, *arXiv:2405.00569*, 2024.

[34] D.M. Shi, On the initial boundary value problem of nonlinear the equation of the moisture in soil, *Acta Math. Appl. Sin.*, **13**:1 (1990), 33–40.

[35] G. Strang, Accurate partial difference methods, *Numer. Math.*, **6**:1 (1964), 37–46.

[36] J.C. Strikwerda, *Finite Difference Schemes and Partial Differential Equations*, SIAM, 2004.

[37] H. Tari and D.D. Ganji, Approximate explicit solutions of nonlinear BBMB equations by He's methods and comparison with the exact solution, *Phys. Lett. A*, **367**:1-2 (2007), 95–101.

[38] D.W. Taylor, *Research on Consolidation of Clays*, Massachusetts Institute of Technology, 1942.

[39] T.W. Ting, A cooling process according to two-temperature theory of heat conduction, *J. Math. Anal. Appl.*, **45**:1 (1974), 23–31.

[40] Q. Xiao and H. Zhao, Nonlinear stability of generalized Benjamin-Bona-Mahony-Burgers shock profiles in several dimensions, *J. Math. Anal. Appl.*, **406**:1 (2013), 165–187.

[41] H. Yin and J. Hu, Exponential decay rate of solutions toward traveling waves for the Cauchy problem of generalized Benjamin-Bona-Mahony-Burgers equations, *Nonlinear Anal. Theory Methods Appl.*, **73**:6 (2010), 1729–1738.

[42] C.-G. Zhu and W.-S. Kang, Numerical solution of Burgers-Fisher equation by cubic B-spline quasi-interpolation, *Appl. Math. Comput.*, **216**:9 (2010), 2679–2686.